Lithos 117 (2010) 229–246

Contents lists available at ScienceDirect

Lithos

journal homepage: www.elsevier.com/locate/lithos

Evolution of lithospheric mantle beneath the Tan-Lu fault zone, eastern North China Craton: Evidence from petrology and geochemistry of peridotite xenoliths

Yan Xiao [a,*], Hong-Fu Zhang [a,*], Wei-Ming Fan [b], Ji-Feng Ying [a], Jin Zhang [a], Xin-Miao Zhao [a], Ben-Xun Su [a]

[a] State Key Laboratory of Lithospheric Evolution, Institute of Geology and Geophysics, Chinese Academy of Sciences, P.O. Box 9825, Beijing 100029, China
[b] Guangzhou Institute of Geochemistry, Chinese Academy of Sciences, P.O. Box 1131, Guangzhou 510640, China

ARTICLE INFO

Article history:
Received 23 October 2009
Accepted 24 February 2010
Available online 6 March 2010

Keyword:
Tan-Lu fault zone
Peridotite xenoliths
Lithospheric mantle
Peridotite–melt interaction
Eastern North China Craton

ABSTRACT

A suite of peridotite xenoliths from Cenozoic Beiyan basalts within the Tancheng-Lujiang (Tan-Lu) wrench fault zone, eastern North China Craton (NCC), has been studied to provide constraints on the nature and evolution of the lithospheric mantle beneath this region. These xenoliths commonly have porphyroclastic, granuloblastic to resorption textures with the absence of coarse-grained texture. They can be subdivided into three types: lherzolite, clinopyroxene (cpx)-rich lherzolite and wehrlite. Lherzolites are characterized by low forsterite contents (Fo) (88–91) in olivines. Whole rock and cpx separates from lherzolites have convex-upward rare earth element (REE) patterns except for one sample which has the highest Fo in olivine and shows a spoon-shaped REE pattern. The Sr–Nd isotopic compositions of cpx separates are depleted, similar to those of mid-ocean ridge basalts (MORB). These geochemical characteristics indicate that the lherzolites represent fragments of newly accreted lithospheric mantle that makes up much of the Late Mesozoic–Cenozoic lithosphere beneath the Tan-Lu fault zone. Cpx-rich lherzolite and wehrlite reflect the interaction of the lithosphere with melt, as evidenced by relatively lower Fo (<87) than the lherzolites (Fo ~ 90), and higher enrichment in cpx and light rare earth elements (LREE). Shallow relics of the Archean cratonic mantle have not been found in this region. Therefore, the abundant cpx-rich lherzolites and wehrlites could be the result of recent modification of lherzolites by asthenospheric melt. The Tan-Lu fault zone facilitated the ascent and migration of asthenospheric melt and enhanced lithospheric mantle—asthenospheric melt reaction. Combined with the data for mantle xenoliths from the adjacent regions, a highly heterogeneous and secular evolution of the lithosphere is inferred beneath the Jiaodong region during Phanerozoic times.

1. Introduction

Refractory mantle roots, often preserved beneath cratons due to their inherent buoyancy and high viscosity, can be modified by more fertile materials through asthenosphere–lithosphere and crust–mantle interactions (Griffin et al., 1998; Zheng et al., 1998; Downes, 2001; O'Reilly et al., 2001; Zhang, 2005; Zhang et al., 2007a; Zheng et al., 2007; Tang et al., 2008). Mantle-derived xenoliths are direct samples of the lithospheric mantle, and can provide direct information about these mantle processes.

The North China Craton (NCC) is one of the oldest cratons on Earth (3.8 Ga) (Liu et al., 1992) and is also one of the major Archean cratons in eastern Eurasia. Previous studies on mantle xenoliths, xenocrysts and solid diamond inclusions in Paleozoic diamondiferous kimberlites from Mengyin County, Shandong Province and Fuxian County, Liaoning Province, show that a thick (~200 km), cold (~40 mW/m^2) and highly refractory lithospheric mantle survived until the mid-Ordovician (Menzies et al., 1993; Harris et al., 1994; Meyer et al., 1994; Zheng et al., 1998; Wang and Gasparik, 2001; Zheng et al., 2001, 2007; Menzies et al., 2007), consistent with the model that Archean crust is underlain by thick, cold and refractory Archean lithospheric mantle (Boyd and Nixon, 1978; Erlank et al., 1987; Griffin et al., 1998; Pearson, 1999; Zhang et al., 2008). However, peridotite xenoliths from the Cenozoic basalts suggest a hot (60–80 mW/m^2), thin (80–60 km) and fertile "younger" lithospheric mantle beneath the eastern NCC (Menzies et al., 1993; Griffin et al., 1998; Zheng et al., 1998; Fan et al., 2000; Hu et al., 2000; Xu, 2001; Zheng et al., 2001; Rudnick et al., 2004; Chu et al., 2009; Zhang et al., 2009a). These observations indicate that the lithospheric mantle of the NCC has not been only considerably thinned but also compositionally changed from highly refractory to more fertile mantle during Phanerozoic times. Systematic investigation of the petrology, mineralogy and Sr–Nd isotopic geochemistry on the spinel lherzolite xenoliths entrained in the Cenozoic basalts of eastern China, show that these lherzolite xenoliths have an "oceanic" affinity and thus may represent newly accreted lithospheric mantle formed by low degree partial melting (Boyd, 1989; Fan et al., 2000). However, more recent studies on mantle xenoliths entrained in the late Mesozoic Junan

* Corresponding authors. No. 19, Beitucheng Xi Road, Chaoyang District, 100029, Beijing, PR China. Tel.: +86 10 82998514; fax: +86 10 62010846.
E-mail addresses: xiaoyan@mail.iggcas.ac.cn (Y. Xiao), hfzhang@mail.iggcas.ac.cn (H.-F. Zhang).

0024-4937/$ – see front matter © 2010 Elsevier B.V. All rights reserved.
doi:10.1016/j.lithos.2010.02.017

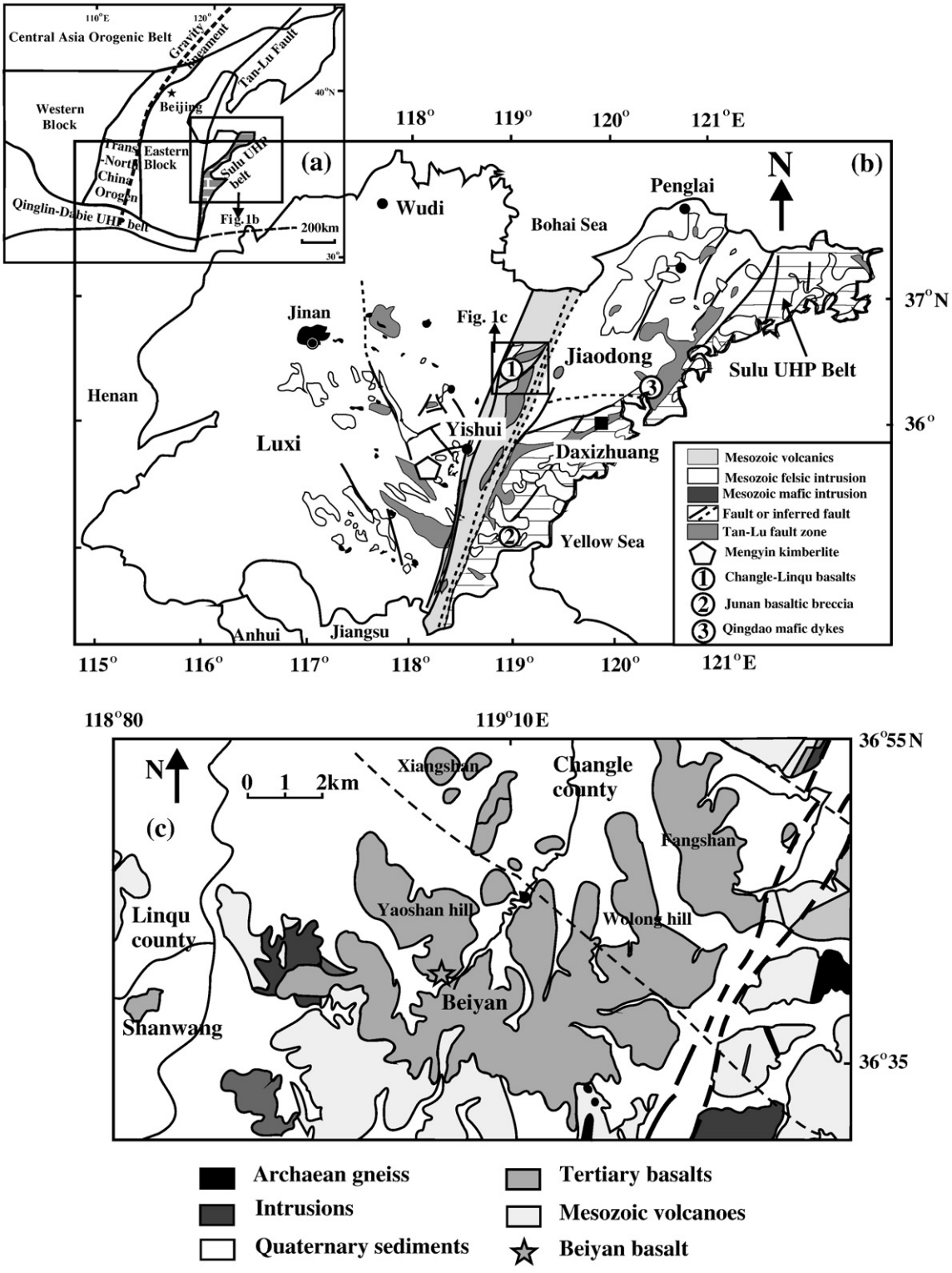

Fig. 1. Simplified geological map showing major tectonic units of the NCC and the xenolith localities mentioned in the text. (a) The tectonic subdivisions of the NCC (after Zhao et al., 2001). (b) Distribution of Mesozoic intrusions and volcanics in Shandong Province, as well as Paleozoic Mengyin diamondiferous kimberlite, with emphasis on basalts and related rocks (after Zhang and Sun, 2002). (c) Distribution of Cenozoic volcanoes in the Changle-Linqu volcanic field (after Wang et al., 2003 and Yang et al., 2009).

basaltic rocks and Qingdao mafic dykes, Shandong Province, show that these volcanic rocks contain two types of mantle peridotite xenoliths, i.e. high-Mg# (Fo>91) and low-Mg# (Fo≤91) peridotite (Ying et al., 2006; Zhang et al., 2009b). Detailed petrological and geochemical studies suggest that the high-Mg# peridotites are samples of the old lithospheric mantle which was severely modified by peridotite–melt interaction, and the low-Mg# peridotites represent fragments of the newly accreted lithospheric mantle. This implies that the newly accreted lithospheric mantle was widespread beneath the eastern NCC in the Late Mesozoic, much earlier than the previous estimate as indicated by the xenoliths entrained in Neogene and Quaternary basalts (Fan et al., 2000; Zheng et al., 2001; Rudnick et al., 2004). In addition, peridotite–melt interaction was also widespread in the Mesozoic lithospheric mantle, as evidenced by Mesozoic basaltic rocks, mantle

Table 1
Modal composition of mantle xenoliths entrained in Beiyan basalts (vol.%).

Sample	Texture	Ol	Opx	Cpx	Sp	Amp	Feld	Ap	Phl
Lherzolite									
CLB05-03	Porphyroclastic	68	18	13	1				
CLB05-13	Porphyroclastic	68	17	14	1				
CLB05-23	Porphyroclastic	68	20	11	1				
CLB05-24	Granuloblastic	76	15	8	1				
CLB05-29	Porphyroclastic	70	18	11	1				
CLB05-30	Porphyroclastic	60	22	17	1		Trace		Trace
CLB05-31	Granuloblastic	75	14	9	2				
CLB05-32	Granuloblastic	75	15	8	2				
CLB05-34	Porphyroclastic	77	15	7	1				
CLB05-47	Porphyroclastic	69	19	11	1				
CLB05-48	Porphyroclastic	68	19	12	1				
CLB05-50	Porphyroclastic	67	18	14	1				
CLB05-51	Porphyroclastic	65	19	15	1				
CLB05-55	Porphyroclastic	63	21	15	1				
Cpx-rich lherzolite									
CLB05-07	Granuloblastic	70	9	20	1			Trace	
CLB05-15	Granuloblastic	70	8	20	2				
CLB05-22	Granuloblastic	70	11	17	2				
CLB05-25	Granuloblastic	66	14	19	1				
CLB05-45	Granuloblastic	70	13	16	1				
CLB05-53	Porphyroclastic	72	9	17	2				
Wehrlite									
CLB05-01	Granuloblastic	72		27	1				
CLB05-02	Granuloblastic	75		24	1				
CLB05-26	Granuloblastic	74		25	1				
CLB05-35	Granuloblastic	73		25	2				
CLB05-46	Granuloblastic	71		28	1	Trace	Trace		
CLB05-80	Resorption texture	75		25					

Note: Ol: olivine; Cpx: clinopyroxene; Opx: orthopyroxene; Sp: spinel; Amp: amphibole; Feld: feldspar; Phl: phlogopite; Ap: apatite.

xenocrysts and xenoliths entrained in the Late Cretaceous volcanic rocks (Zhang et al., 2002, 2003; Zhang, 2005; Ying et al., 2006; Zhang et al., 2007b, 2009a). Thus, the evolution of the lithospheric mantle beneath the eastern NCC is complicated and the mantle has experienced widespread peridotite–melt interaction, perhaps during both the Mesozoic and Cenozoic. The objectives of this paper are to further constrain the evolution of newly accreted lithospheric mantle since the late Mesozoic and to describe the reaction processes recorded in the mantle-derived xenoliths.

This paper focuses on a suite of the newly discovered mantle peridotite xenoliths from the Beiyan locality of the Cenozoic Changle-Linqu volcanic field within the Tan-Lu fault zone in Shandong Province, eastern NCC. The petrological and geochemical data reported in this paper are used to probe the nature and evolution of the lithospheric mantle beneath the Tan-Lu fault region, and the processes involved in its evolution. Previously published mantle xenolith data (Xu et al., 1996b, 1998; Zheng et al., 1998; Ying et al., 2006; Zheng et al., 2007; Zhang et al., 2009b) have been incorporated for comparison, and to demonstrate the modification of the newly accreted lithospheric mantle.

2. Geological background

The NCC is bounded by the Central Asia Orogenic belt to the north and the Qinling–Dabie–Sulu high–ultrahigh pressure metamorphic belt to the south, which separates the craton from the Yangtze Block (Fig. 1a). The craton has been divided into three blocks, i.e. a Western Block, a Trans-North China Orogen and an Eastern Block, based on geology, geochronology, tectonic evolution and P–T-t paths for the metamorphic rocks (Zhao et al., 2001) (Fig. 1a). The Western Block consists of Late Archean to Paleoproterozoic metasedimentary belts that unconformably overlie the Archean basement (Zhao et al., 2001). The Trans-North China Orogen is a Proterozoic orogenic belt that

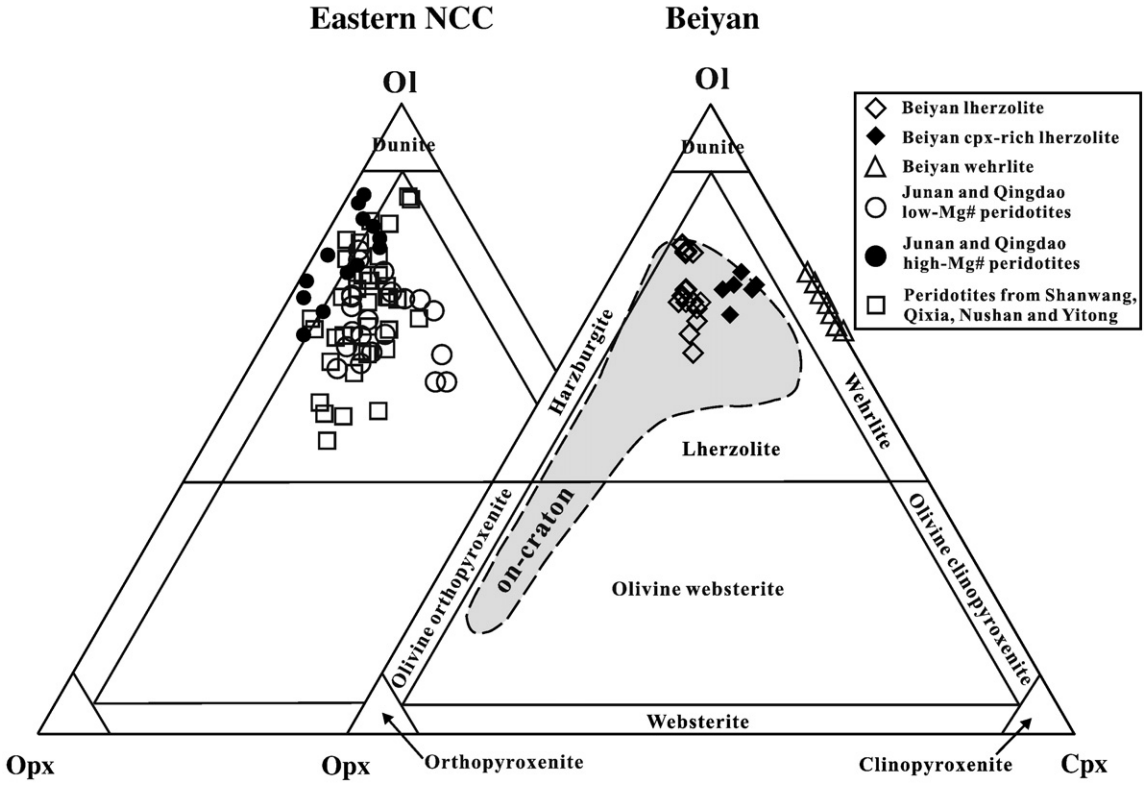

Fig. 2. Petrological classification of mantle xenoliths from the Beiyan locality. The on-craton Cenozoic mantle xenoliths in eastern China are from Fan et al. (2000). The data of Shanwang, Qixia, Nüshan, Yitong, Qingdao and Junan are from Zheng et al. (1998), E and Zhao (1987), Zhang et al. (2009b), Ying et al. (2006).

amalgamated the Archean Western Block and Eastern Block into an integrated craton. The orogen comprises Late Archean to Paleoproterozoic tonalitic–trondhjemitic–granodioritic (TTG) gneisses and granitoids that are interleaved with abundant sedimentary and volcanic rocks which developed in magmatic arc and intra-arc basin environments (Zhao et al., 2001). The basement of the Eastern Block is primarily composed of Early to Late Archean TTG gneisses and 2.5 Ga syntectonic granitoids, with Early to Late Archean granitic gneisses and supracrustal rocks.

Unlike other Archean cratons worldwide, the NCC has experienced widespread tectonothermal reactivation during Phanerozoic times. Kimberlites were emplaced during the Ordovician (Chi and Lu, 1996; Zhang and Yang, 2007). After a long magmatic hiatus, volcanism resumed in the Late Jurassic and intensified in the Early Cretaceous and Cenozoic as shown by the emplacement of voluminous Early Cretaceous volcanic rocks, alkaline and granitoid rocks (Fan et al., 2000; Xu, 2001; Zhang and Sun, 2002; Zhang et al., 2004, 2005) and extensive Tertiary to Neogene basalts carrying abundant mantle and crustal xenoliths (Zhou and Armstrong, 1982; Cao and Zhu, 1987; Zheng et al., 1998; Tang et al., 2006). These magmas and their entrained mantle and crustal xenoliths provide us with an opportunity to understand the evolution of the subcontinental lithosphere beneath the eastern NCC.

Shandong Province is situated in the central part of the eastern NCC and is separated by the Tan-Lu fault into two parts: the western Luxi part and the eastern Jiaodong part. Jiaodong differs from the Luxi due to the occurrence of the Sulu ultrahigh pressure metamorphic belt. Cenozoic volcanism in Shandong Province is distributed in the Changle-Linqu, Yishui, Penglai, Qixia and Wudi fields (Chen and Peng, 1985; E and Zhao, 1987; Wang et al., 1987; Zheng et al., 1998) (Fig. 1b). The Changle-Linqu (10.6–18.8 Ma) and Yishui (12.1–14.0 Ma) (Jin, 1985) volcanoes occur within the Tan-Lu fault zone. The Penglai (5.6 Ma) and Qixia (6.2 Ma) (Jin, 1985) volcanoes cover the Jiaodong Group metamorphic rock in eastern Shandong and the Wudi volcano in northwestern Shandong. Volcanoes in eastern Shandong erupted in the Miocene (11–19 Ma) and in western Shandong in the Pliocene (5–8 Ma) with the youngest volcano (0.7 Ma) in Wudi (Chen and Peng, 1985). The Cenozoic basalts in Shandong Province are dominantly composed of alkali olivine basalts, olivine nephelinites and basanites (Chen and Peng, 1985; Xu et al., 2000). Hundreds of Cenozoic volcanoes distributed in the Changle and Linqu counties (Fig. 1c) and basalts in the Changle-Linqu volcanic field directly overlie the Early Tertiary coal-bearing lacustrine sedimentary rocks of the Wutu Formation (Wang et al., 2003). Beiyan volcano is one of the volcanoes in the Changle-Linqu volcanic field and is next to the Shanwang volcano (Zheng et al., 1998) (Fig. 1c).

The Tan-Lu fault zone is a major wrench fault in northeastern Asia and extends from Nikolayevsk in Russia to the Yangtze Craton in South China with a strike length of more than 5000 km (Xu et al.,

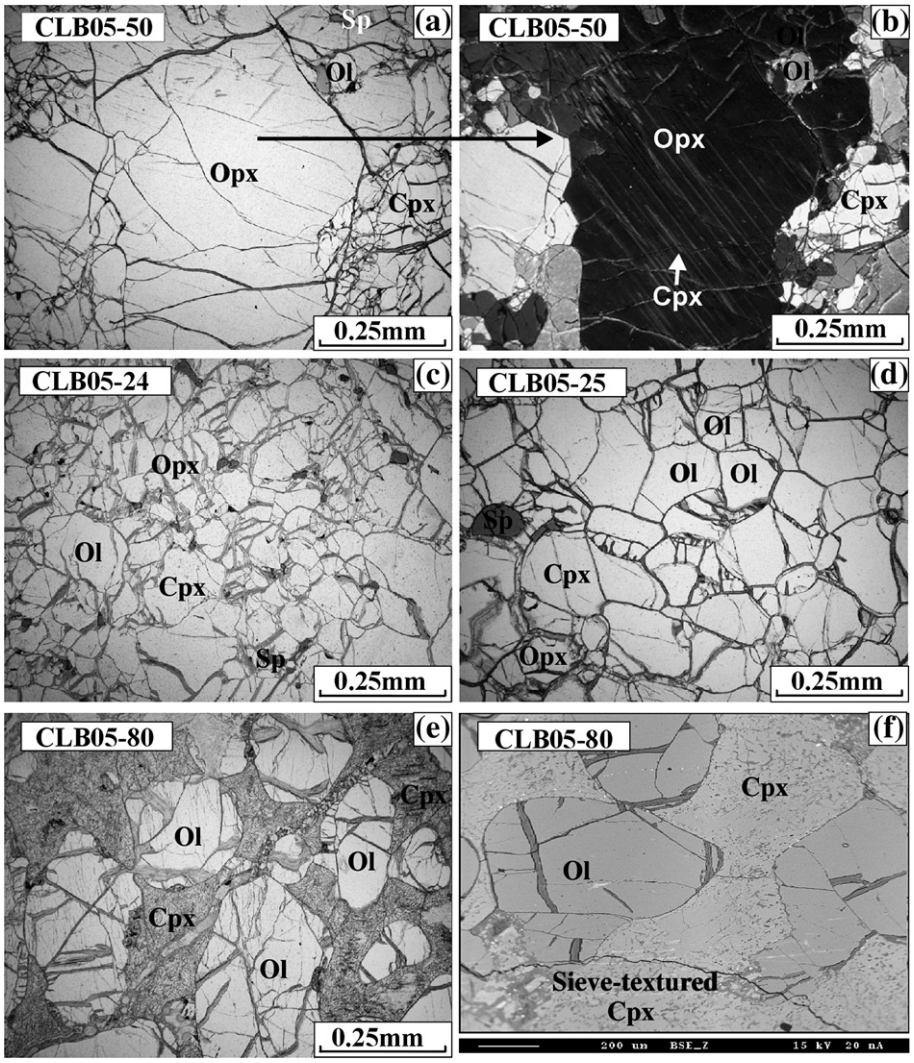

Fig. 3. Photomicrographs and backscattered electron micrographs of representative texture of the Beiyan peridotites. (a) and (b) Porphyroclastic texture. (c) and (d) Granuloblastic texture. (e) and (f) Resorption texture. (a), (c), (d) and (e) are plane-polarized light. (b) is cross-polarized light.

1987, 1993; Zheng et al., 1998). This fault cuts through the eastern part of the NCC. Previous studies (Peng et al., 1986; Fan and Hooper, 1989; Xu et al., 1993, 1996a; Zheng et al., 1998, 2007) show that this fault extends deep into the lithospheric mantle. It may therefore have influenced lithospheric mantle evolution.

3. Xenolith petrography

The Beiyan alkaline basalts contain abundant deep-seated xenoliths of dominantly spinel lherzolites and wehrlites with minor pyroxenites and megacrysts of augite and anorthoclase. The peridotite xenoliths are very fresh and large (10–15 cm in diameter). Most peridotite xenoliths are unfoliated or weakly foliated. Beiyan peridotite xenoliths can be subdivided into three types: lherzolite, cpx-rich lherzolite and wehrlite, which can also be recognized in other xenolith suites of the eastern NCC such as Shanwang, Qixia, Nüshan, Yitong, Fuxin, Qingdao and Junan (Table 1 and Fig. 2) (E and Zhao, 1987; Zheng et al., 1998; Ying et al., 2006; Zheng et al., 2007; Zhang et al., 2009b). The Beiyan peridotite xenoliths are highly enriched in cpx, different from normal xenoliths from other basaltic localities worldwide.

The texture of ultramafic mantle xenoliths worldwide can be divided into coarse-grained (representing undeformed mantle with coarse grains (>4 mm), curved and indented grain boundaries and large anhedral spinels), porphyroclastic and granuloblastic textures according to the grain sizes and the deformation and recrystallization features (Downes, 1990). The textures of mantle xenoliths within the Tan-Lu fault, such as the Beiyan locality, have their own characteristics. Due to strong deformation and recrystallization, they have complex features (Fig. 3) and mainly show porphyroclastic and granuloblastic textures.

3.1. Porphyroclastic texture

Porphyroclastic texture occurs only in the Beiyan lherzolite and cpx-rich lherzolite and is characterized by the occurrence of large-grained orthopyroxene (opx) porphyroclasts (>1 mm) surrounded by small neoblasts (≤0.5 mm) (Fig. 3a and b). Beiyan lherzolites with porphyroclastic texture are often foliated and generally contain <10% opx porphyroclasts. The opx porphyroclasts often show fractures, curved or zigzag grain boundaries and are commonly strained. Some of them show fine exsolution lamellae of cpx and sometimes they contain small and rounded olivine inclusions (Fig. 3b), suggesting that these small olivine grains are crystallized prior to opx recrystallization. Olivine and cpx occur as small neoblasts which are strain-free recrystallized grains (Fig. 3a and b). Some deformed olivine neoblasts also show undulatory extinction or asymmetric extinction and kink bands. Rare spinel typically occurs as interstitial and vermicular-shaped crystals, and is sometimes included in opx.

3.2. Granuloblastic texture

The granuloblastic texture occurs in the Beiyan peridotites. Peridotites with granuloblastic texture are strongly tectonized with a grain-refined fabric, and are often tabular with abundant triple junctions and straight grain boundaries (Downes, 1990). All the minerals in the granuloblastic peridotites belong to the same generation and are recrystallized (Fig. 3c and d). They display equilibrated texture with nearly 120° triple junctions and curved grain boundaries (Fig. 3d). The grain sizes are relatively fine from 0.2 mm to 0.5 mm. Some deformed grains show undulatory extinction and kink bands. Cpx in most lherzolites have rims with sieve texture (Fig. 4a, b, c). In some samples, the opx was clearly replaced by cpx (Fig. 4d).

3.3. Resorption texture

An unusual resorption texture occurs in mantle xenoliths from Beiyan, especially in the wehrlite xenoliths. In sample CLB05-80, all the cpx have sieve texture and occur as interstitial grains between

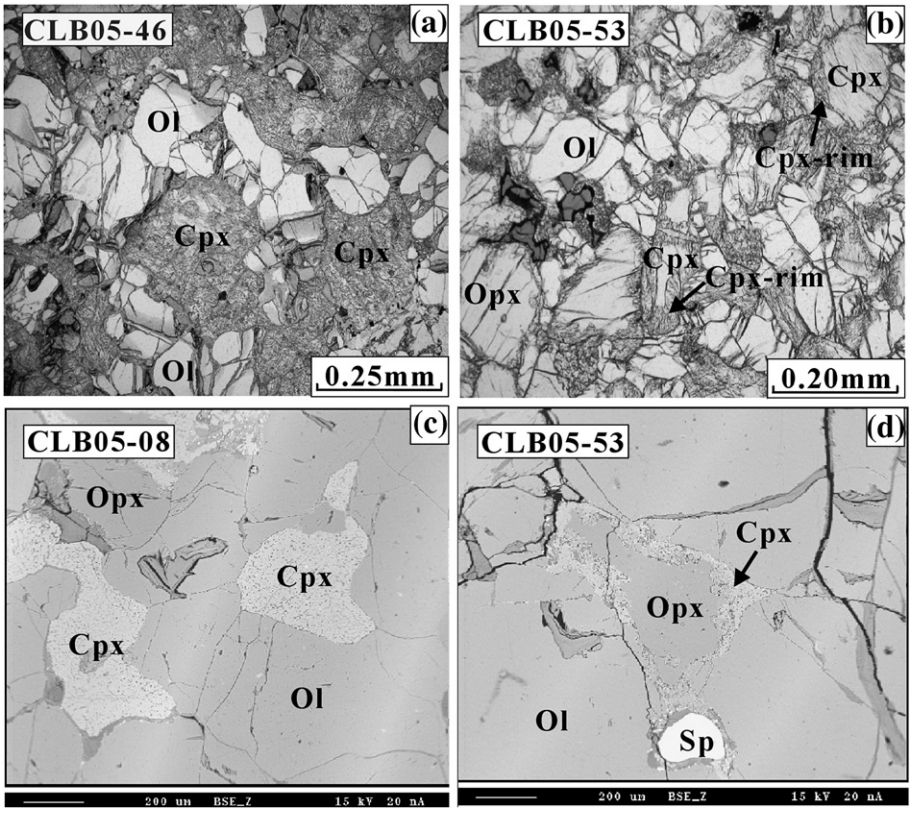

Fig. 4. Photomicrographs (plane-polarized light) and backscattered electron micrographs of sieve-textured cpx from the Beiyan xenoliths.

rounded olivine crystals with xenomorphic granular texture (Fig. 3e and f). This may suggest that the sieve-textured cpx formed at the expense of primary olivine and opx through peridotite–melt reaction. The interstitial sieve-textured cpx and rounded olivine form a resorption texture (Fig. 3e and f).

In addition, a few metasomatic minerals such as mica, apatite, amphibole, feldspar and calcite also occur in the Beiyan peridotites (Fig. 5a–d). Phlogopite occurs as a vein in sample CLB05-30 and shows zigzag grain boundaries surrounded by small minerals such as olivine and cpx (Fig. 5a and b), suggesting multiple metasomatic events. Apatite, amphibole and feldspar crystals rarely occur in microcracks or on the boundaries of olivine and pyroxenes (Fig. 5c and d). Feldspar occurs in the reaction zone as a matrix of anhedral grains in which other secondary minerals are embedded (Fig. 5d). Calcite is relatively common in the Beiyan peridotites and occurs mainly as veins (Fig. 5e and f).

4. Analytical methods

After thin-section observation representative lherzolite and wehrlite xenoliths were selected and crushed to <30 mesh. Cpx separates were carefully handpicked under a binocular microscope to a purity of >99%. The cpx was cleaned in an ultrasonic bath in distilled water and then leached with purified dilute HCl before isotopic analysis.

Modal mineralogy of the peridotites was determined by point counting techniques (Table 1). Major element compositions of minerals (Table 2) were determined with a Cameca SX50 electron microprobe at the Institute of Geology and Geophysics (IGG), Chinese Academy of Sciences. Analyses were carried out with a beam of 15 keV and 10 nA and focused to a spot of ~2 μm diameter. Natural mineral standards were used for calibration and the PAP correction procedure was applied to the data (Pouchou and Pichoir, 1991).

For trace element analyses, whole rocks and cpx separates (100 mg) were weighed and dissolved in distilled $HF–HNO_3$ in 15 ml Savillex Teflon screw-cap capsules at 100 °C for 2 days, dried and then digested with 6 M HCl at 150 °C for 4 days. Dissolved samples were diluted to 100 ml before analyses. A blank solution was prepared and the total procedural blanks were <50 ng for all the trace elements reported in this paper (Table 3). Three duplicates and two standards were prepared using the same procedure to monitor the analytical reproducibility. Trace elements were analyzed with an Elan 6100 DRC ICP-MS at IGG. The discrepancy between the triplicates is less than 5% for all the elements given in Table 3. Analyses of standards are in agreement with the recommended values.

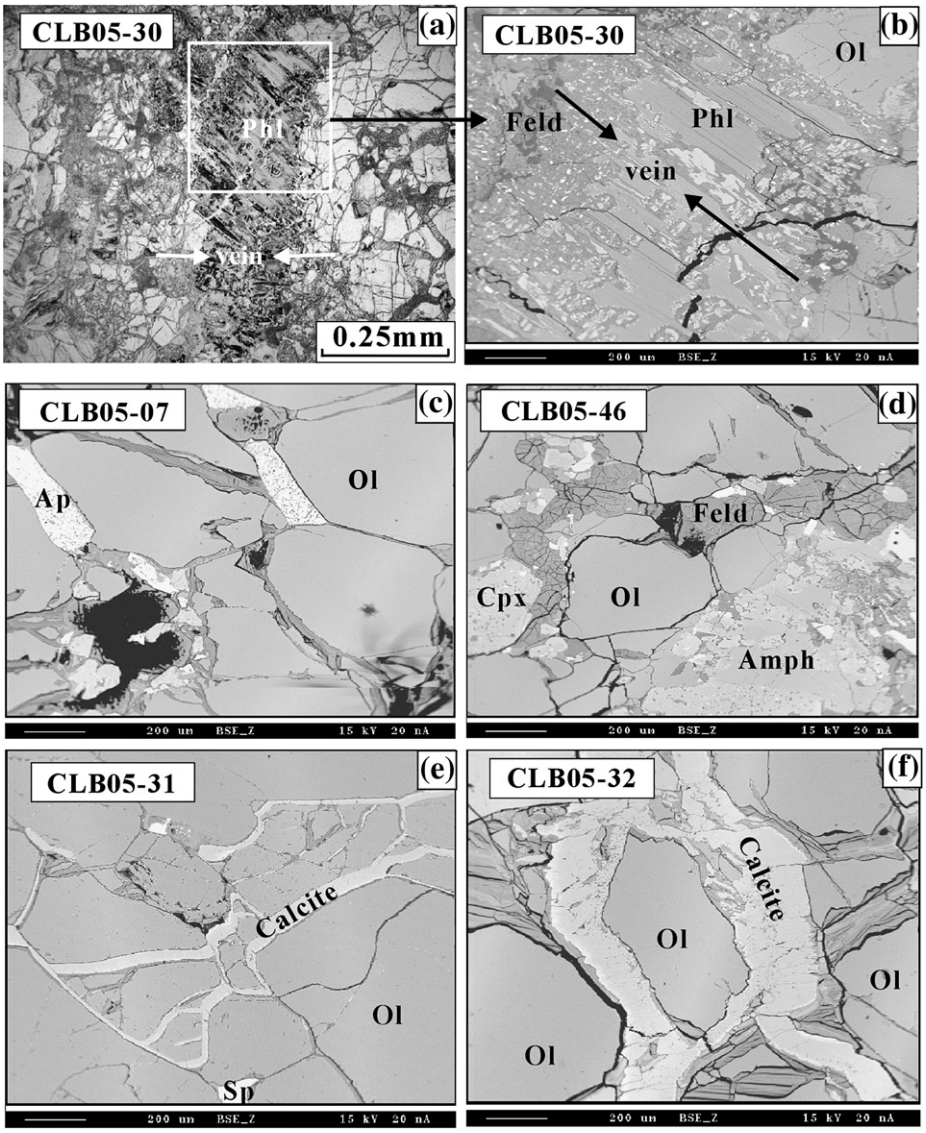

Fig. 5. Photomicrographs (plane-polarized light) and backscattered electron micrographs of metasomatic minerals and carbonate veins.

For Sr and Nd isotope analyses, cpx separates were rinsed several times in deionised water after leaching with sub-boiling distilled 6 M HCl for 30 min. Then they were powdered with an agate mill to 200 mesh. About 100 mg of sample powder was weighed out and a known quantity of mixed ^{84}Sr, ^{85}Rb, ^{149}Sm and ^{145}Nd spike solution was added to each sample. Samples were digested in Teflon beakers with a mixture of concentrated HF and HNO_3 at 150 °C for 7 days. The decomposed samples were then dried on a hot plate and the residue was re-dissolved and dried down with $HClO_4$ to remove the HF. The dried salts were dissolved again in 1 ml of dilute HCl and then loaded onto columns containing AG50W-X8 resins for separation and purification of Rb, Sr and REE, with the REE cut finally loaded on to HDEHP columns for separation of Nd and Sm, using HCl eluants. Nd and Sr isotopic compositions were determined using a Finnigan MAT-262 thermal ionization mass spectrometer at IGG. The mass fractionation corrections for Sr and Nd isotope ratios were based on $^{86}Sr/^{88}Sr = 0.1194$ and $^{146}Nd/^{144}Nd = 0.7219$. Repeat analyses yielded $^{87}Sr/^{86}Sr$ of 0.710245 ± 0.000011 for the NBS-987 standard and $^{143}Nd/^{144}Nd$ of 0.511853 ± 0.000012 for the La Jolla standard. The results are given in Table 4.

5. Analytical results

5.1. Mineral chemistry

Multiple analyses on the cores and the rims of the constituent minerals, olivine, opx and cpx show that all the mineral phases are homogeneous within and between grains. The average compositions of the minerals are reported in Table 2.

5.1.1. Olivine

Olivine from the Beiyan peridotites is low in MgO and NiO and high in FeO and MnO contents, leading to extremely low Fo contents, especially for cpx-rich lherzolites and wehrlites (Table 2 and Fig. 6a, b). Although olivine compositions from lherzolite, cpx-rich lherzolite and wehrlite overlap, their Fo contents decrease from 91.0 to 88.8 in lherzolites identical to late Mesozoic–Cenozoic peridotites (Zheng et al., 1998; Ying et al., 2006; Zhang et al., 2009b), from 87.6 to 82.2 in cpx-rich lherzolites, then from 86.9 to 81.0 in wehrlites. The highest Fo numbers observed in the Beiyan peridotites are similar to those in the low-Mg# (≤91) peridotites in Junan, but not the high-Mg# (>91) peridotites (Ying et al., 2006; Zhang et al., 2009b). The extremely low Fo (<87) olivine in the Beiyan cpx-rich lherzolites and wehrlites have also been observed in mantle peridotitic xenoliths along the Tan-Lu fault zone at Shanwang (Wang et al., 1987; Zheng et al., 1998), Nüshan (Xu et al., 1998) and Fuxin (Zheng et al., 2007). At Beiyan, the NiO content decreases from lherzolites (0.32–0.47 wt.%) to cpx-rich lherzolites (0.31–0.41 wt.%) and to wehrlites (0.19–0.37 wt.%) accompanied by a decrease in Fo (Table 2 and Fig. 6b). In general, the Beiyan lherzolites fall into the field of Cenozoic peridotites (Fig. 6a), but cpx-rich lherzolites and wehrlites plot far from the field of Cenozoic peridotites.

5.1.2. Opx

Opx occurs only in lherzolites and cpx-rich lherzolites, but not in wehrlites. They have low-Mg# (83.8–91.4), Al_2O_3 (2.22–4.63 wt.%) and CaO (0.19–0.87 wt.%) contents and show a decreasing trend from lherzolites to cpx-rich lherzolites. Such a compositional feature broadly corresponds to that of the coexisting olivine, suggesting a general equilibrium between olivine and opx. No significant variation between large porphyroclasts and fine-grained ones has been observed (Table 2).

5.1.3. Cpx

Cpxs from the Beiyan lherzolites and cpx-rich lherzolites are generally bright emerald-green Cr-diopsides and from wehrlites they are dark green diopsides. They have relatively low-Mg# (<92) and wide compositional ranges in Al_2O_3 (2.77–8.73 wt.%), Cr_2O_3 (0.07–1.50 wt.%), TiO_2 (0.04–2.36 wt.%) and Na_2O (0.69–2.05 wt.%) (Table 2). Al_2O_3 contents in these cpx show a good correlation with Mg# numbers from lherzolites to cpx-rich lherzolites to wehrlites (Fig. 6c), but their TiO_2 contents are relatively scattered (TiO_2 vs. Mg# plot, Fig. 6d). In addition, the exsolution lamellae and sieve-textured cpx rims have slightly higher Al_2O_3 and TiO_2 contents compared with the clean cores (Table 2).

5.1.4. Spinel

Spinel from the Beiyan xenoliths is characterized by large compositional variability such as Cr# (1.67–41.8) and Al_2O_3 contents (31.9–62.1 wt.%) (Table 2 and Fig. 6e–f). Most Beiyan peridotite spinels plot within the field for Cenozoic peridotites (Fig. 6e). The Cr# in spinel is positively correlated with the Mg# in cpx (Fig. 6f).

5.1.5. Metasomatic minerals

Phlogopite occurs as a vein in sample CLB05-30 and has Mg# (88.3) and major element compositions similar to that found in the phlogopite-bearing lherzolites in Hannuoba, Sanyitang and Hebi (Zhao et al., 2007). One amphibole grain was found in the wehrlite CLB05-46 and is pargasite with high TiO_2, resembling amphibole from peridotite xenoliths from the NCC (Zheng et al., 2001). Feldspars that occur in association with the amphibole in sample CLB05-46 are sanidines, which have rarely been reported in mantle peridotites (Xu et al., 1996b). The carbonate minerals in these peridotites are calcites. Dolomites have not been found. Peridotites with carbonate veins do not show a big difference in major elements and trace element compositions compared to those without carbonate veins.

5.2. Trace element concentrations

In anhydrous spinel-facies mantle peridotites, cpx is a main repository of trace elements and its trace element composition can be used in the petrogenetic interpretation of mantle processes (Rampone et al., 1991; McDonough et al., 1992). However, some peridotites in Beiyan are hydrous and trace element concentrations of cpx alone may not be enough to represent the whole rock situation. So, trace element compositions of whole rock and cpx separates from the Beiyan peridotites are reported in Table 3.

5.2.1. Lherzolites and cpx-rich lherzolites

The whole rock and cpx separates from the Beiyan lherzolites and cpx-rich lherzolites display a large variation in trace element abundances and chondrite-normalized rare earth element (REE) patterns ($\sum$REE = 4.62–84.7 ppm and $(La/Yb)_N = 1.58–20.2$ in whole rocks and $\sum$REE = 19.6–103 ppm and $(La/Yb)_N = 0.91–6.54$ in cpx separates) (Table 3 and Fig. 7). Three types of chondrite-normalized REE patterns occur in lherzolites and cpx-rich lherzolites.

(1). Spoon-shaped REE pattern: lherzolite CLB05-31 with the highest Fo is characterized by a spoon-shaped REE pattern with Eu or Pr at the minimum in both the whole rock and cpx (Fig. 7a). This sample shows low REE abundances and LREE/HREE fractionation both in the whole rock and cpx separates ($(La/Yb)_N = 1.58$ and 0.91, respectively). Apart from La-Pr slight enrichment, this cpx shows a depletion in middle rare earth elements (MREE), which is similar to the LREE-depleted patterns of cpx in the Junan low-Mg# peridotites (Fig. 7b). In primitive mantle-normalized trace element diagrams, cpx separates show significantly negative Ba and slightly negative HFSE, (i.e. Nb, Zr, and Hf) and Ti anomalies, but the whole rock exhibits negative Ti and positive Sr and Pb anomalies (Fig. 7b).

(2). LREE-enriched and convex-upward REE patterns: most lherzolites and cpx-rich lherzolites from Beiyan display LREE-enriched

Table 2
Representative electron microprobe analyses (wt.%) of minerals from Beiyan mantle xenoliths.

Sample	CLB05-03				CLB05-07				CLB05-13				CLB05-15			
Rock	Sp lherzolite				Sp cpx-rich lherzolite				Sp lherzolite				Sp cpx-rich lherzolite			
Mineral	Ol	Cpx	Opx	Sp	Ol	Cpx	Opx	Sp	Ol	Cpx	Opx	Sp	Ol	Cpx	Opx	Sp
SiO_2	41.4	53.8	56.7		40.7	52.2	55.6		41.0	53.2	55.9		39.7	49.9	53.9	
TiO_2		0.20	0.08	0.37		0.33		0.55		0.38	0.02	0.08		0.62	0.16	0.33
$Al2O_3$		3.60	3.04	45.9		2.91	2.76	31.9		6.05	4.25	54.1		7.11	4.43	54.5
Cr_2O_3		0.96	0.54	21.0		1.50	0.42	34.1		0.90	0.37	13.6		0.74	0.29	10.2
FeO	10.9	2.89	6.63	13.9	11.7	3.22	7.79	17.4	9.97	2.27	6.14	10.9	16.9	4.80	10.5	17.7
MnO	0.14	0.10	0.15	0.03	0.21	0.08	0.22	0.23	0.18	0.12	0.09	0.11	0.25	0.09	0.22	0.11
MgO	47.9	16.5	32.7	17.7	46.2	16.1	31.8	15.4	48.5	15.0	32.7	19.9	43.5	14.3	30.1	17.2
CaO	0.05	20.4	0.75		0.04	22.3	0.68		0.07	20.3	0.62		0.08	19.1	0.67	
Na2O		1.34	0.10			0.69	0.13			1.96	0.12			1.84	0.06	
NiO	0.37	0.07	0.10	0.35	0.32	0.02	0.11	0.19	0.38	0.02	0.19	0.24	0.31	0.06	0.12	0.36
Total	101	99.9	101	99.3	99.2	99.4	99.4	99.8	100	100	100	98.9	101	98.6	100	100
Mg#	88.8	91.1	89.9	69.6	87.6	90.0	88.0	61.5	89.7	92.3	90.6	76.7	82.2	84.2	83.7	63.7
Cr#				23.5				41.8				14.5				11.2

Sample	CLB05-29					CLB05-30				
Rock	Sp lherzolite					Sp lherzolite				
Mineral	Ol	Cpx	Opx(P)	Opx(N)	Sp	Ol	Cpx	Opx	Sp	Pl
SiO_2	41.0	52.4	56.9	56.7		41.1	52.0	54.7		38.1
TiO_2		0.49	0.08	0.08	0.06		0.56	0.13	0.18	5.93
Al_2O_3		5.14	2.92	2.70	52.1		6.84	4.52	56.7	16.7
Cr_2O_3		0.90	0.33	0.29	16.0		0.71	0.30	10.0	0.37
FeO	10.0	2.51	6.40	6.33	11.5	10.6	4.00	7.85	13.3	4.98
MnO	0.16	0.11	0.16	0.16	0.08	0.13	0.01	0.12	0.09	0.03
MgO	48.4	15.4	33.4	33.6	19.2	48.0	14.8	31.3	19.0	20.4
CaO	0.04	22.3	0.36	0.38		0.03	19.5	0.69		0.02
Na_2O		1.17	0.03	0.03			1.82	0.07		0.85
NiO	0.32	0.03	0.07	0.09	0.26	0.35	0.12	0.16	0.38	0.17
K_2O										8.66
Total	100	100	101	100	99.2	100	100	99.8	99.6	96.1
Mg#	89.7	91.7	90.4	90.5	75.1	89.1	86.9	87.8	72.0	88.3
Cr#					17.1				10.6	

Sample	CLB05-34				CLB05-45				CLB05-47					CLB05-48				
Rock	Sp lherzolite				Sp cpx-rich lherzolite				Sp lherzolite					Sp lherzolite				
Mineral	Ol	Cpx	Opx	Sp	Ol	Cpx	Opx	Sp	Ol	Cpx	Opx(P)	Opx(N)	Sp	Ol	Cpx	Opx(P)	Opx(N)	Sp
SiO_2	39.8	52.6	55.0		39.8	50.4	54.9		40.0	51.3	54.2	54.3		41.1	52.7	54.4	54.6	
TiO_2		0.17	0.04			0.55	0.13	0.34		0.55	0.09	0.06	0.12			0.13	0.14	0.02
Al_2O_3		4.10	3.08	42.9		5.93	3.61	41.9		6.93	4.63	4.60	58.3		6.08	4.44	4.25	59.1
Cr_2O_3		1.16	0.46	26.7		1.29	0.56	25.1		0.83	0.37	0.34	9.32		0.81	0.41	0.30	9.89
FeO	8.78	2.11	5.76	12.7	10.1	3.50	6.68	14.5	10.9	2.98	6.75	6.73	11.2	10.2	3.12	6.52	6.50	10.1
MnO	0.13	0.06	0.18	0.09	0.06	0.05	0.11	0.16	0.11	0.06	0.14	0.13	0.13	0.15	0.05	0.14	0.15	0.04
MgO	49.3	15.5	34.0	17.7	48.4	15.3	32.9	17.5	48.0	14.9	32.1	32.2	20.4	48.1	16.3	32.6	32.8	20.7
CaO	0.02	22.1	0.41		0.07	19.4	0.74		0.06	19.8	0.71	0.68		0.02	19.2	0.46	0.44	
Na_2O		1.57	0.09			1.95	0.14			1.88	0.10	0.11			1.65	0.07	0.06	
NiO	0.47	0.03	0.07	0.23	0.36	0.02	0.13	0.23	0.38	0.07	0.08	0.03	0.36	0.35	0.04	0.10	0.12	0.38
Total	98.5	99.3	99.1	100	98.8	98.4	99.9	99.6	99.5	99.2	99.2	99.2	99.8	100	100	99.2	99.4	100
Mg#	91.0	92.9	91.4	71.5	89.6	88.7	89.9	68.5	88.8	90.0	89.5	89.6	76.7	89.5	90.4	90.0	90.1	78.7
Cr#				29.4				28.7					9.69					10.1

Sample	CLB05-01			CLB05-02			CLB05-26		
Rock	Sp wehrlite			Sp wehrlite			Sp wehrlite		
Mineral	Ol	Cpx	Sp	Ol	Cpx	Sp	Ol	Cpx	Sp
SiO_2	40.3	49.1		39.3	49.5		39.7	50.9	
TiO_2		2.36	0.59		2.08	0.65		1.28	0.72
Al_2O_3		4.94	36.3		7.35	50.0		7.54	48.7
Cr_2O_3		1.48	29.6		0.32	13.7		0.28	12.6
FeO	12.6	3.40	18.1	18.1	4.23	19.9	17.7	5.27	21.4
MnO	0.21	0.08	0.23	0.21	0.11	0.15	0.21	0.09	0.22
MgO	46.4	14.7	15.4	42.8	13.7	15.3	42.7	13.9	15.8
CaO	0.13	22.7		0.08	22.1		0.08	19.9	
Na_2O		0.80			0.99			1.35	
NiO	0.37	0.03	0.26	0.21	0.04	0.24	0.24	0.03	0.27
K_2O									
Total	99.9	99.6	100	101	100	99.9	101	101	99.7
Mg#	86.9	88.6	60.5	81.0	85.4	58.1	81.3	82.6	57.0
Cr#			35.4			15.6			14.8

CLB05-22				CLB05-23				CLB05-24				CLB05-25			
Sp cpx-rich lherzolite				Sp lherzolite				Sp lherzolite				Sp cpx-rich lherzolite			
Ol	Cpx	Opx	Sp	Ol	Cpx	Opx	Sp	Ol	Cpx	Opx	Sp	Ol	Cpx	Opx	Sp
40.3	51.7	54.5		40.8	52.8	55.5		41.0	53.6	56.1		40.4	52.3	54.5	
	0.66	0.01	0.42		0.43	0.12	0.30		0.04	0.07			0.45	0.08	0.16
	6.33	3.57	46.1		5.45	3.89	46.6		2.77	2.22	33.8		6.75	4.32	56.3
	1.21	0.47	19.8		1.27	0.49	19.5		1.02	0.40	34.6		0.68	0.27	9.59
13.7	4.06	8.88	17.0	12.3	3.59	7.73	15.3	8.84	2.17	5.83	14.1	13.0	3.40	7.81	14.4
0.19	0.18	0.30	0.19	0.12	0.13	0.11	0.08	0.14	0.05	0.17	0.19	0.18	0.07	0.17	0.13
45.4	14.6	30.7	16.5	46.9	15.1	31.8	17.6	49.4	16.5	34.2	16.1	45.7	14.6	31.2	18.4
0.06	19.4	0.75		0.06	20.2	0.87		0.02	22.7	0.50		0.03	19.0	0.64	
	1.99	0.11			1.36	0.08			1.07	0.02			2.05	0.12	
0.37	0.09	0.13	0.25	0.39	0.13	0.04	0.31	0.41	0.04	0.02	0.18	0.41	0.07	0.08	0.35
100	100	99.4	100	101	100	101	99.7	100	100	100	98.9	100	99.4	99.2	99.3
85.6	86.6	86.2	63.6	87.3	88.4	88.1	67.5	91.0	93.2	91.4	67.3	86.4	88.6	87.8	69.6
			22.3				21.9				40.7				10.2

CLB05-31				CLB05-32			
Sp lherzolite				Sp lherzolite			
Ol	Cpx	Opx	Sp	Ol	Cpx	Opx	Sp
41.2	53.0	55.6		40.1	51.9	54.5	
	0.17	0.03	0.10		0.11	0.02	0.02
	4.51	3.43	45.6		4.18	3.43	49.6
	1.11	0.50	23.3		1.06	0.41	19.9
9.18	2.34	5.75	11.6	9.18	2.35	5.92	10.5
0.14	0.11	0.13	0.14	0.13	0.09	0.15	0.08
49.6	15.9	33.5	18.5	49.5	16.3	33.8	19.3
0.06	21.3	0.65		0.04	22.2	0.42	
	1.40	0.06			0.90	0.02	
0.40	0.07	0.11	0.31	0.40		0.01	0.31
101	100	100	99.5	99.4	99.1	98.7	100
90.7	92.4	91.3	74.2	90.7	92.6	91.1	76.7
			25.5				21.2

CLB05-50						CLB05-51					CLB05-53				CLB05-55				
Sp lherzolite						Sp lherzolite					Sp cpx-rich lherzolite				Sp lherzolite				
Ol	Cpx	Cpx*	Opx(P)	Opx(N)	Sp	Ol	Cpx	Opx(P)	Opx(N)	Sp	Ol	Cpx	Opx	Sp	Ol	Cpx	Opx(P)	Opx(N)	Sp
41.3	51.4	51.0	54.9	55.2		40.2	52.3	55.2	55.6		40.4	51.1	55.8		40.4	52.2	55.1	55.1	
	0.70	0.76	0.11	0.11	0.07		0.74	0.16	0.18	0.13		0.91	0.09	0.04		0.58	0.15	0.19	0.12
	6.73	7.00	4.15	3.59	58.2		6.26	3.89	3.66	54.6		6.34	3.88	55.7		6.41	3.66	3.75	59.1
	0.86	0.80	0.38	0.27	11.5		0.79	0.40	0.34	12.9		0.52	0.37	13.7		0.80	0.31	0.32	10.5
10.0	2.45	2.54	6.65	6.66	10.0	10.4	2.69	6.74	6.91	11.2	12.9	3.36	6.85	11.7	10.6	2.66	6.8	6.81	11.0
0.16	0.06	0.06	0.13	0.13	0.14	0.17	0.12	0.16	0.19	0.15	0.18	0.06	0.20	0.09	0.14	0.12	0.15	0.18	0.09
47.9	14.3	14.2	32.3	32.6	20.1	48.0	14.6	33.0	33.2	19.4	45.7	14.1	32.7	19.0	47.5	14.4	32.4	32.4	19.0
0.01	21.1	21.1	0.55	0.45		0.06	21.1	0.19	0.38		0.06	22.1	0.44		0.02	21.1	0.40	0.45	
	1.76	1.75	0.07	0.09			1.84	0.06	0.05			1.36	0.07			1.77	0.05	0.06	
0.39	0.05	0.03	0.07	0.04	0.36	0.35	0.05	0.05	0.09	0.39	0.33	0.05	0.09	0.36	0.38	0.10	0.08	0.02	0.38
100	99.4	99.1	99.4	99.2	100	99.1	101	99.8	101	98.8	100	100	101	101	99.1	100	99.1	99.3	100
89.6	91.3	90.9	89.7	89.8	78.3	89.3	90.7	89.8	89.7	75.6	86.4	88.3	89.6	74.5	89.0	90.7	89.6	89.5	75.7
					11.7					13.7				14.2					10.6

CLB05-35			CLB05-46					CLB05-80	
Sp wehrlite			Sp wehrlite					Wehrlite	
Ol	Cpx	Sp	Ol	Cpx	Sp	Amp	Feld	Ol	Cpx
39.6	48.7		40.9	48.9		42.8	51.6	40.2	49.2
	1.67			2.31	0.33	3.46	0.09		1.94
	8.73	62.1		6.50	46.1	14.5	23.2		6.93
	0.07	1.58		1.39	20.5	1.71			0.42
17.1	4.89	17.1	12.6	3.20	14.9	4.83	0.10	15.6	4.45
0.25	0.11	0.07	0.23	0.07	0.20	0.08	0.01	0.21	0.13
42.6	13.2	18.4	46.4	14.6	17.2	15.7	0.04	43.3	14.0
0.05	20.7		0.11	21.8		10.5	5.12	0.24	21.6
	1.44			0.71		3.09	1.22		1.05
0.19	0.01	0.35	0.31	0.04	0.30	0.10	0.02	0.24	0.04
						1.48	6.58		
99.8	99.5	99.6	101	99.5	99.5	98.3	88.0	99.7	99.8
81.7	83.0	65.9	86.8	89.2	67.6	85.4		83.3	85.0
		1.67			23.0				

Table 3
Trace element abundances (ppm) of whole rock and clinopyroxene seperates from Beiyan xenoliths.

Rock	Sp cpx-rich lherzolite						Sp lherzolite				Sp wehrlite						Wehrlite	
Sample	CLB05-07		CLB05-22		CLB05-25		CLB05-30		CLB05-31		CLB05-01		CLB05-35		CLB05-46		CLB05-80	
	WH	Cpx	WH	Cpx	WH	Cpx	WH	Cpx	WH	Cpx	WH	Cpx	WH	Cpx	WH	Cpx	WH	Cpx
Rb	3.54	0.67	1.02	0.22	1.41	0.28	3.00	0.46	1.25	0.13	2.79	5.58	2.73	2.32	2.17	1.72	2.38	2.57
Ba	27.3	3.25	13.5	0.65	19.1	0.69	44.5	2.21	16.9	0.19	20.2	94.4	23.0	17.0	24.1	21.1	24.6	16.9
Sr	513	340	208	187	105	106	190	174	230	24.6	216	391	612	145	344	164	285	224
Y	6.73	12.2	2.27	12.3	4.37	14.1	4.82	19.9	1.88	8.66	4.28	18.4	4.52	11.1	4.92	13.2	5.04	10.6
Zr	36.3	17.0	10.7	30.1	18.8	16.6	24.5	55.3	10.8	5.12	22.5	110	24.7	54.0	27.2	56.8	32.7	59.0
Nb	6.93	0.54	1.00	1.56	1.84	0.74	4.26	1.89	1.29	0.95	2.88	17.8	3.37	6.26	3.17	4.59	5.38	6.75
La	18.2	14.0	1.12	9.42	2.13	5.30	2.45	9.79	0.44	1.34	1.72	15.5	3.44	9.04	3.20	7.66	2.97	6.99
Ce	32.0	30.8	2.90	24.7	5.10	11.6	6.30	27.4	0.79	2.15	5.70	38.7	7.53	18.8	8.27	22.4	7.37	16.1
Pr	3.80	3.56	0.41	3.38	0.69	1.38	1.03	4.17	0.09	0.23	1.01	5.69	1.02	2.44	1.30	3.39	1.07	2.20
Nd	14.5	13.7	1.78	15.0	3.10	5.94	4.58	20.5	0.37	1.21	4.73	27.8	4.40	11.8	5.68	17.1	4.80	10.8
Sm	2.83	2.68	0.45	3.20	0.81	1.59	1.22	5.05	0.10	0.49	1.28	6.75	1.21	3.25	1.46	4.04	1.37	2.83
Eu	0.70	0.88	0.11	1.00	0.22	0.61	0.35	1.55	0.03	0.21	0.36	2.17	0.37	1.05	0.39	1.35	0.42	1.00
Gd	2.25	2.39	0.37	2.94	0.72	1.99	1.05	4.71	0.14	0.86	1.09	5.86	1.12	3.18	1.15	3.61	1.23	3.04
Tb	0.33	0.39	0.06	0.43	0.13	0.39	0.17	0.76	0.03	0.20	0.17	0.88	0.18	0.53	0.19	0.55	0.20	0.48
Dy	1.59	2.23	0.34	2.56	0.84	2.67	1.02	4.17	0.24	1.53	0.95	4.48	1.04	2.77	1.08	2.94	1.15	2.60
Ho	0.29	0.48	0.07	0.48	0.18	0.58	0.21	0.82	0.06	0.35	0.18	0.80	0.20	0.49	0.22	0.57	0.22	0.47
Er	0.71	1.39	0.20	1.36	0.50	1.68	0.53	2.15	0.19	1.04	0.45	1.95	0.49	1.21	0.55	1.43	0.54	1.18
Tm	0.01	0.21	0.03	0.20	0.07	0.27	0.07	0.30	0.03	0.15	0.06	0.25	0.06	0.17	0.08	0.20	0.07	0.15
Yb	0.61	1.45	0.21	1.31	0.46	1.76	0.45	2.00	0.19	1.00	0.33	1.45	0.35	0.97	0.45	1.31	0.40	0.95
Lu	0.09	0.20	0.03	0.18	0.07	0.25	0.07	0.28	0.03	0.14	0.05	0.19	0.05	0.13	0.06	0.17	0.06	0.14
Hf	0.81	0.65	0.26	0.58	0.50	0.66	0.63	1.56	0.26	0.20	0.52	2.63	0.76	1.82	0.78	1.70	0.94	1.89
Pb	1.11	0.49	0.52	0.23	0.71	0.34	0.56	0.13	0.60	0.11	0.54	0.49	0.67	0.32	0.73	0.17	0.71	0.36
Ti	680	2847	309	3962	1039	2679	2000	3380	176	947	723	3081	2955	11771	1029	5124	2613	27618
Ta	0.32	0.16	0.06	0.28	0.11	0.17	0.25	0.27	0.05	0.11	0.12	1.62	0.19	0.51	0.20	0.56	0.39	0.68
Th	1.24	0.72	0.08	0.29	0.20	0.39	0.14	0.37	0.08	0.17	0.05	1.47	0.38	0.86	0.17	0.22	0.26	0.51
U	0.37	0.15	0.02	0.08	0.04	0.12	0.03	0.08	0.01	0.05	0.03	0.18	0.17	0.26	0.04	0.07	0.07	0.15
$\sum$REE	84.7	86.5	10.4	78.5	19.4	50.1	24.3	103	4.62	19.6	22.3	131	26.0	67.0	29.0	79.8	26.9	59.5
$(La/Yb)_N$	20.2	6.54	3.69	4.87	3.17	2.04	3.72	3.33	1.58	0.91	3.56	7.27	6.64	6.31	4.84	3.97	5.11	4.99

The subscript *N* denotes the chondrite-normalized element ratio (Anders and Grevesse, 1989). WH: whole rock; Cpx: clinopyroxene separates.

Table 4
Sr and Nd isotopic data for clinopyroxene separates in Beiyan mantle xenoliths.

Sample	Rock	Rb ppm	Sr ppm	$^{87}Rb/^{86}Sr$	$^{87}Sr/^{86}Sr \pm 2\sigma$	Sm ppm	Nd ppm	$^{147}Sm/^{144}Nd$	$^{143}Nd/^{144}Nd \pm 2\sigma$	εNd
CLB05-07	Sp cpx-rich lherzolite	0.80	319	0.0073	0.703133±13	1.88	9.66	0.1179	0.512974±12	6.55
CLB05-22	Sp cpx-rich lherzolite	0.20	164	0.0035	0.703177±12	2.07	9.78	0.1282	0.512894±13	4.99
CLB05-25	Sp cpx-rich lherzolite	0.28	91.9	0.0087	0.703038±13	1.01	3.98	0.1533	0.513035±13	7.75
CLB05-30	Sp lherzolite	0.43	155	0.0081	0.703118±13	3.33	14.4	0.1399	0.512942±13	5.94
CLB05-31	Sp lherzolite	0.14	23.4	0.0170	0.703419±13	0.35	0.83	0.2591	0.513391±07	14.7
CLB05-01	Sp wehrlite	5.35	437	0.0354	0.703260±13	6.19	25.9	0.1443	0.512948±13	6.05
CLB05-35	Sp wehrlite	2.33	150	0.0448	0.703159±13	2.33	8.17	0.1725	0.512951±10	6.10
CLB05-46	Sp wehrlite	1.85	172	0.0311	0.703180±12	3.92	13.9	0.1702	0.512927±13	5.64
CLB05-80	Wehrlite	2.36	258	0.0265	0.703305±11	2.75	7.71	0.2160	0.512965±09	6.38

and convex-upward REE patterns both in whole rock and cpx separates with high LREE/HREE fractionation ($(La/Yb)_N = 3.17–3.72$ and 2.04–4.87, respectively) (Table 3 and Fig. 7c). In primitive mantle-normalized trace element diagrams, the pattern for the whole rock shows positive Ba, Sr and Pb anomalies and negative HFSE (e.g. Zr, Hf, and Ti) anomalies, whereas cpx displays negative anomalies in Ba and HFSE (e.g. Nb, Zr, and Ti) (Fig. 7d). In general, these lherzolites have coupled trace element patterns between the whole rocks and their cpx separates, showing that most trace elements reside in cpx.

(3). Highly LREE-enriched REE patterns: cpx-rich lherzolite CLB05-07 shows highly LREE-enriched REE patterns both in the whole rock and cpx separate ($(La/Yb)_N = 20.2$ and 6.54, respectively) (Fig. 7e). The whole rock has identical REE abundances in L-MREEs as that of the corresponding cpx (Fig. 7e), perhaps due

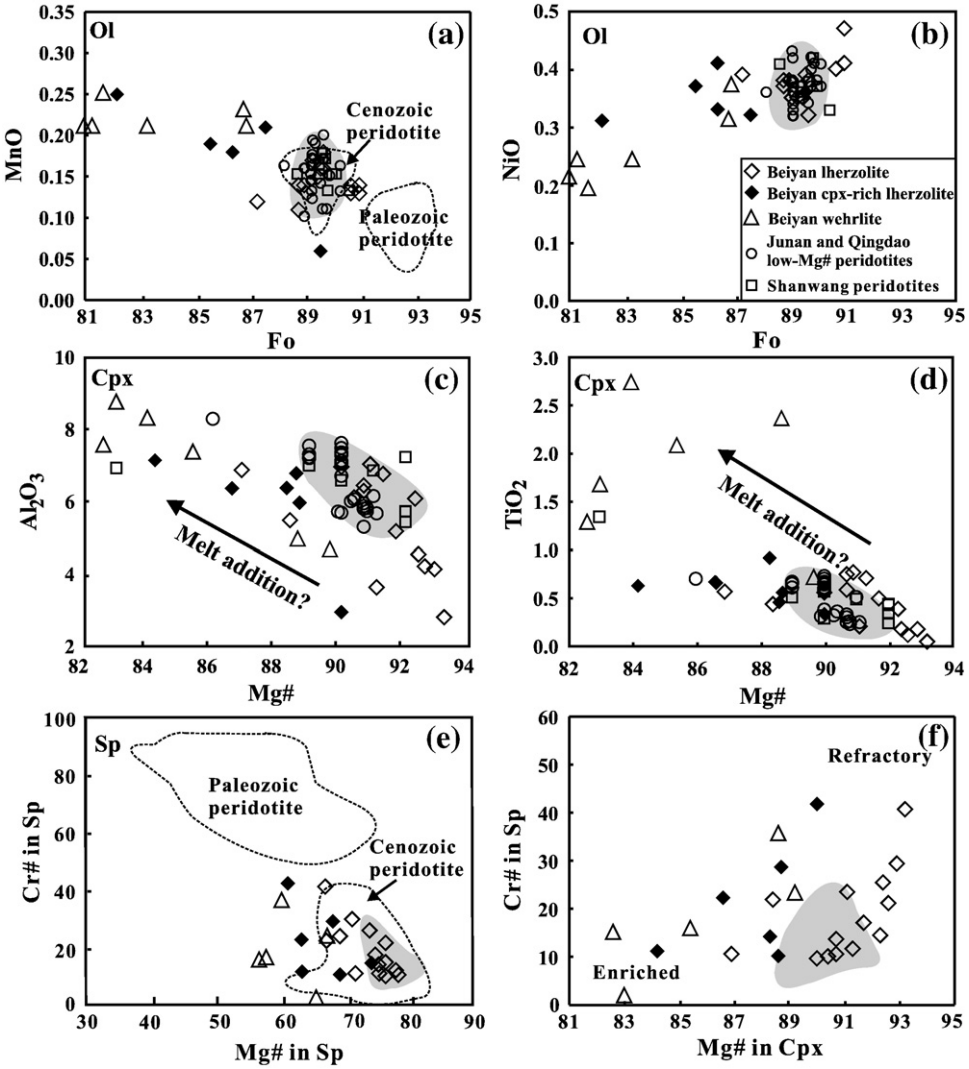

Fig. 6. Mineral compositions for the Beiyan peridotites compared with published data from eastern NCC. Data sources: Qingdao (Zhang et al., 2009b); Junan (Ying et al., 2006); Shanwang (Zheng et al., 1998); fields for the Paleozoic and Cenozoic peridotites are after Zheng et al. (2001); Paleozoic and Cenozoic peridotites are from Zheng et al. (1998, 2001) and Ying et al. (2006).

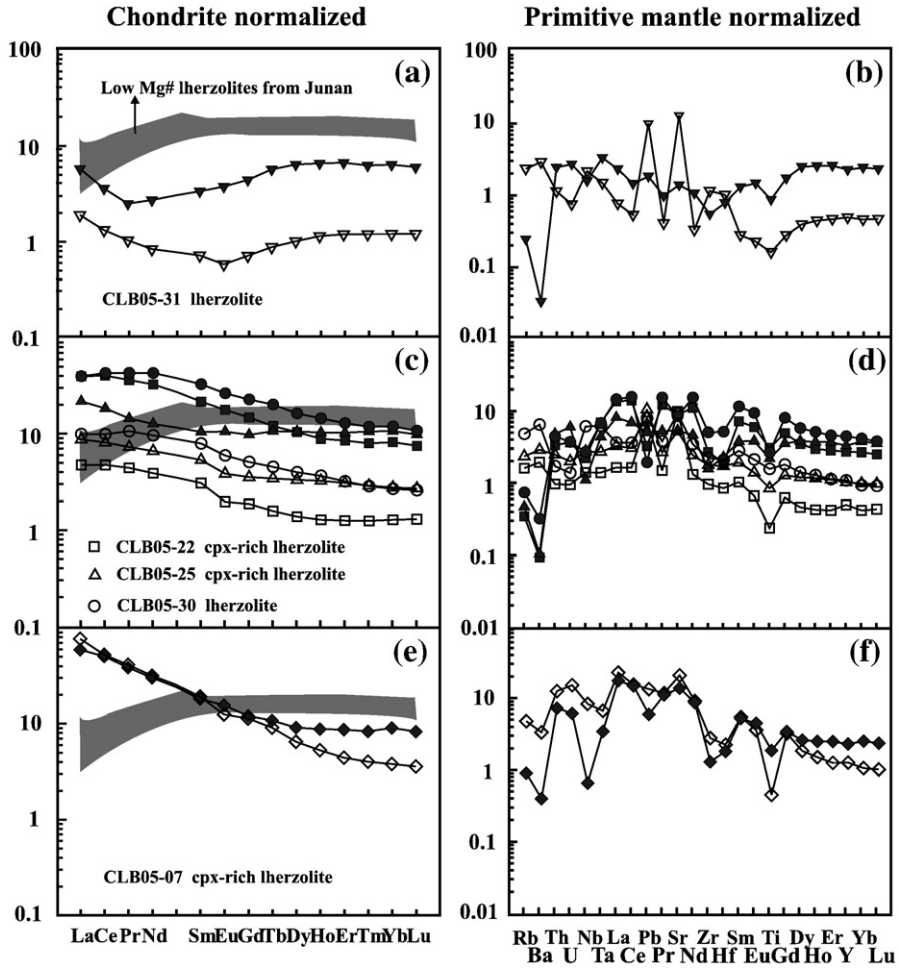

Fig. 7. Whole rock and cpx chondrite-normalized REE patterns and primitive mantle-normalized trace element spidergrams for the Beiyan lherzolites. Chondrite and primitive mantle values are from Anders and Grevesse (1989) and Sun and McDonough (1989), respectively. The shaded area represents cpxs from Junan low-Mg# peridotites (Ying et al., 2006). Open and solid symbols represent whole rock and cpx separates, respectively.

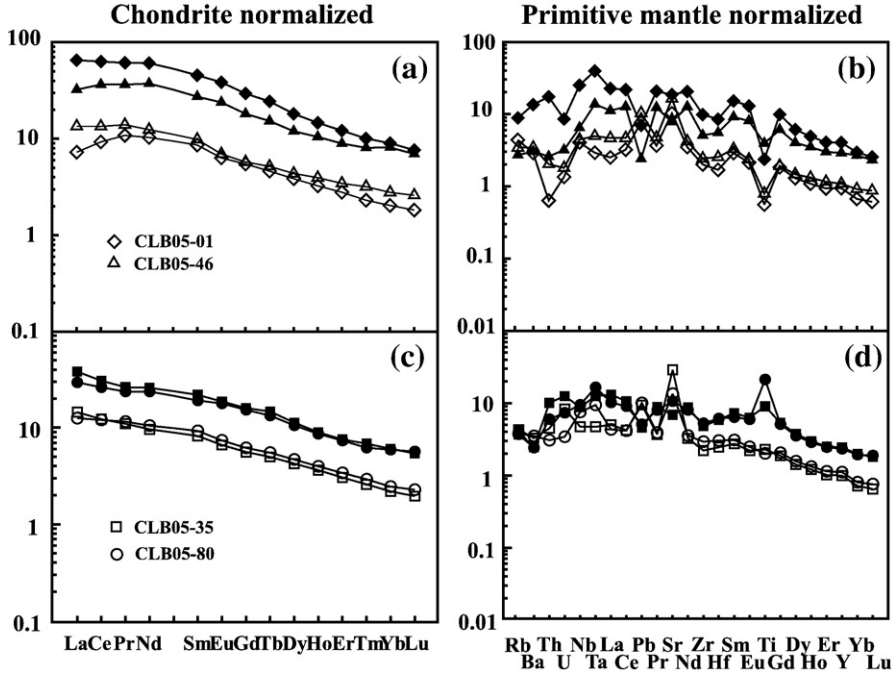

Fig. 8. Whole rock and cpx chondrite-normalized REE patterns and primitive mantle-normalized trace element spidergrams for the Beiyan wehrlites. Chondrite and primitive mantle values are from Anders and Grevesse (1989) and Sun and McDonough (1989), respectively. Open and solid symbols represent whole rock and cpx separates, respectively.

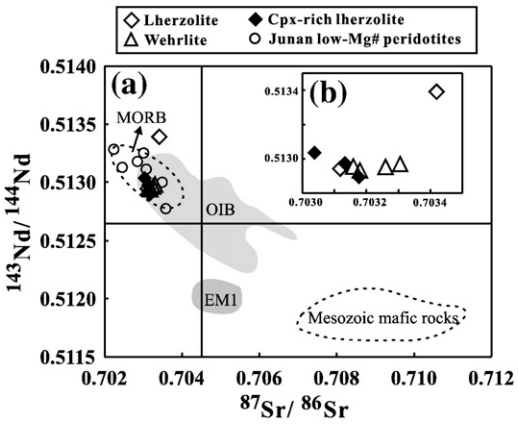

Fig. 9. $^{87}Sr/^{86}Sr$ vs.$^{143}Nd/^{144}Nd$ diagram for cpx from the Beiyan xenoliths. MORB, OIB and EM1 components are from Zindler and Hart (1986). The data for the Junan peridotites are from Zhang et al. (2009b). The fields for Paleozoic kimberlites and peridotites and Mesozoic mafic rocks are from Zhang et al. (2002).

to the presence of apatite with high LREE in this sample. In primitive mantle-normalized trace element diagrams, both the whole rock and cpx separate display negative Ba, high field strength element (HFSE, i.e. Nb, Ta, Zr, and Hf) and Ti anomalies (Fig. 7f), although a positive Sr anomaly is present in whole rock.

5.2.2. Wehrlites

Whole rock and cpx in Beiyan wehrlites show similar highly LREE-enriched and convex-upward REE patterns (Table 3 and Fig. 8a and c). Whereas LREE/HREE fractionations are very similar both in whole rock and cpx separates ($(La/Yb)_N = 3.56–6.64$ and 3.97–7.27, respectively), the cpx separates contain 3–5 times the REE concentrations of the whole rocks ($\sum REE = 22.3–29.0$ ppm in whole rock and 59.5–131 ppm in cpx separates). These wehrlites also have higher REE concentrations and LREE/HREE fractionations than the lherzolites, indicating a sequential evolution of wehrlites from lherzolites with melt addition. In primitive mantle-normalized trace element diagrams (Fig. 8b and d), whole rocks exhibit positive Pb and Sr anomalies and negative Ti anomaly, but cpx separates show negative anomalies for HFSE (e.g. Zr, and Hf) and Pb. Cpx from two samples (CLB05-35 and CLB05-80) have positive Ti anomalies.

5.3. Sr and Nd isotopes

The Beiyan peridotites have relatively homogeneous Sr–Nd isotopic compositions ($^{87}Sr/^{86}Sr = 0.7030–0.7034$ and $^{143}Nd/^{144}Nd = 0.5129–0.5134$) (Table 4 and Fig. 9). Most samples fall within the field of MORB, with one sample (CLB05-31) plotting above the MORB field. This lherzolite has the highest Mg# minerals and a much higher Nd isotopic ratio than other samples, although the Sr isotopic ratio is only slightly enriched (Fig. 9). Sr–Nd isotopic compositions of cpx from other Beiyan peridotites are identical to those from the Late Cretaceous Junan low-Mg# lherzolite xenoliths and Cenozoic lherzolite xenoliths from eastern China.

6. Discussion

6.1. Beiyan peridotites: remnants of newly accreted lithospheric mantle

Three Late Cretaceous xenolith-bearing basaltic volcanic fields, i.e. 67 Ma Junan basaltic breccias (Ying et al., 2006), 74 Ma Daxizhuang basaltic lava flows (Yan et al., 2003) and 82 Ma Qingdao mafic dikes (Zhang et al., 2009b), have recently been found within the Sulu ultrahigh pressure metamorphic belt in the Jiaodong region, east of the Tan-Lu Fault (Fig. 1b). Detailed petrological and in-situ trace element geochemical investigation of mantle xenoliths entrained in them has revealed the existence of two types of peridotites: high-Mg# (Fo>91)

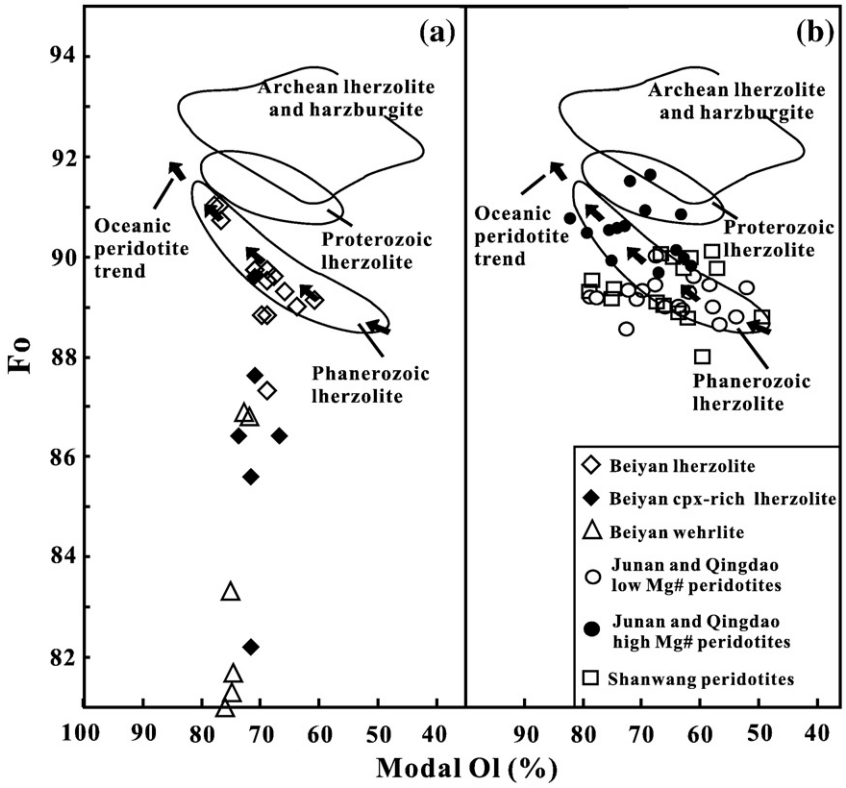

Fig. 10. Fo vs. modal (%) of olivines from the Beiyan mantle xenoliths. Archean, Proterozoic and Phanerozoic fields are from Griffin et al. (1999). Oceanic trend is after Boyd (1989). Data for the Shanwang, Junan and Qingdao peridotites are from Zheng et al. (1998), Ying et al. (2006), and Zhang et al. (2009b).

peridotites and low-Mg# (Fo≤91) peridotites (Ying et al., 2006; Zhang et al., 2009b). High Mg# peridotites are mainly harzburgites and cpx-poor lherzolites (Fig. 2). They are high in olivine Fo (Fo>91) and spinel Cr# and enriched in LREE and Sr–Nd isotopes (Zhang et al., 2009b). Low-Mg# peridotites are lherzolites (Fig. 2) with low olivine Fo (Fo≤91) and spinel Cr# and depleted LREE and Sr–Nd isotopic compositions, completely different from the high-Mg# peridotites. These geological characteristics indicate that the high-Mg# peridotites represent the relics of the ancient Archean lithospheric mantle, while the low-Mg# lherzolites are interpreted to be fragments of newly accreted lithospheric mantle (Ying et al., 2006; Zhang et al., 2009b). These observations indicate that not only did large scale lithospheric thinning occur beneath the eastern NCC, but also locally lithospheric accretion occurred in the late Mesozoic.

It is widely accepted that the major elements of mantle xenoliths such as olivine Fo and olivine mode are very useful in distinguishing Archean and Phanerozoic mantle xenoliths (Boyd, 1989). In the plot of olivine mode vs. olivine Fo, the Beiyan lherzolites fall within the field for Phanerozoic lherzolite xenoliths (Griffin et al., 1998) and have an "oceanic" trend (Boyd, 1989), similar to the Junan and Qingdao low-Mg# peridotites (Fig. 10). No high-Mg# peridotitic xenoliths were found in Beiyan. The lherzolite CLB05-31 with the highest Fo (90.7) found in Beiyan has olivine Fo similar to that of low-Mg# lherzolites from Junan, but still not up to the high-Mg# peridotites (Fig. 10). This lherzolite has a spoon-shaped REE pattern, resembling the LREE-depleted patterns in Junan low-Mg# peridotites (Fig. 7a). The depletion of MREE relative to Junan low-Mg# peridotites may be due to slightly higher initial melt extraction. The spoon-shaped pattern indicates that the lherzolite could be produced by chromatographic reaction between a metasomatic agent and a refractory mantle peridotite (Navon and Stolper, 1987; Bodinier et al., 1990). Other Beiyan lherzolites with Fo (87–90) have similar mineral compositions to Cenozoic peridotite xenoliths from the localities in the eastern NCC, such as Yitong, Shanwang and Nüshan (Fig. 6). The convex-upward REE patterns of these lherzolites and low Fo provide unequivocal evidence for mantle metasomatism relative to lherzolite CLB05-31 and Junan low-Mg#

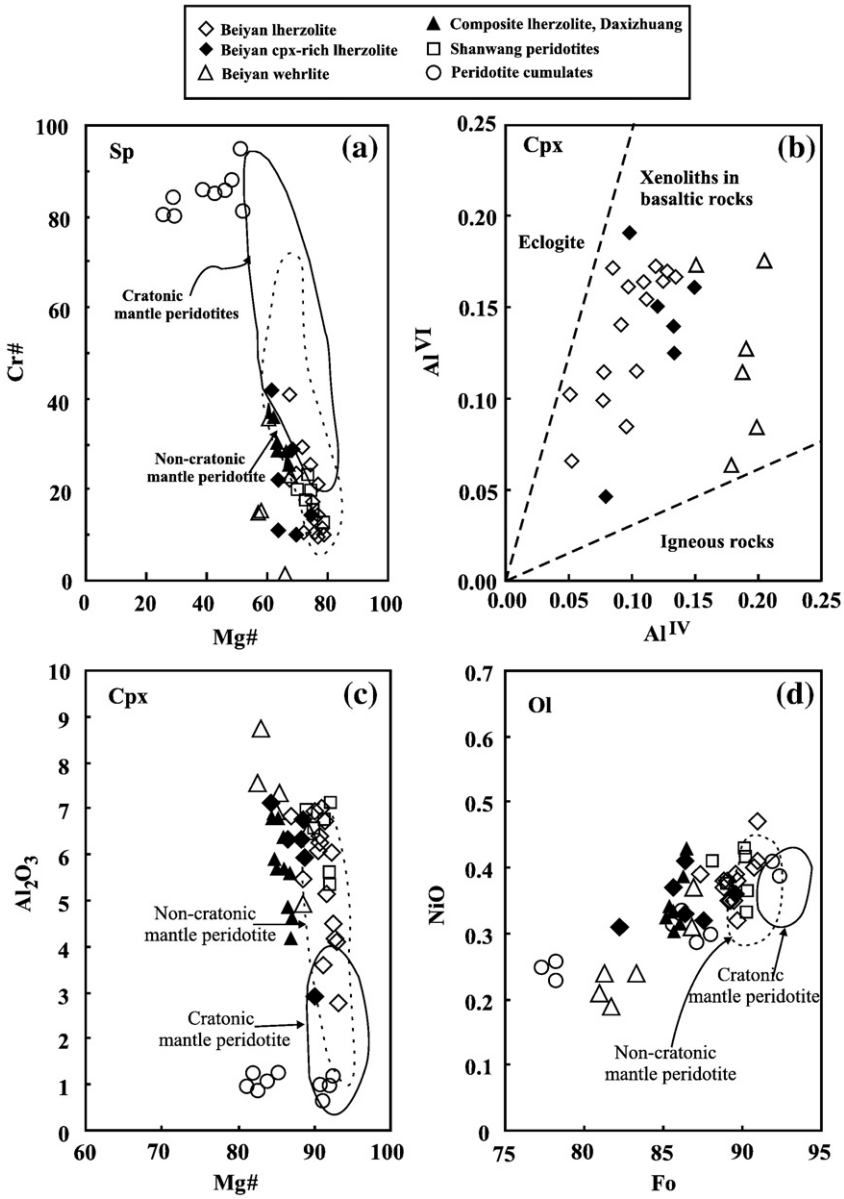

Fig. 11. Plots of Mg# vs. Cr# (a) in spinel, Al^{IV} vs. Al^{VI} in cpx (b), Mg# vs. Al_2O_3 (c) in cpx, Fo vs. NiO (d) in olivine from the Beiyan xenoliths. Data for Ecolgite, xenoliths in basaltic rocks and igneous rocks are from Aoki and Kushiro (1968). Fields of cratonic and non-cratonic mantle peridotites worldwide and data for cumulates are from Walter (2003). Data for Shanwang peridotites and Daxizhuang composite xenolith are from Zheng et al. (1998),and Zhang et al. (2007a).

peridotites. These features indicate that the Beiyan lherzolites are fragments of newly accreted lithopheric mantle.

In addition, cpx-rich lherzolites with extremely low Fo (<87) fall far below the Phanerozoic lherzolite field in the modal olivine vs. Fo plot and exhibit highly LREE-enriched patterns (Figs. 7c, e and 10). They also show a trend in mineral compositions with lherzolites (Fig. 6). We suggest that recent asthenospheric melt–peridotite reaction is the cause, as proposed from the studies on mantle olivine xenocrysts and a highly-fertile lherzolite xenolith from the Mesozoic–Cenozoic basalts (Zhang, 2005; Ying et al., 2006; Tang et al., 2008; Zhang et al., 2009b).

6.2. Origin of Beiyan wehrlites

Wehrlites are subordinate to lherzolites and harzburgites in the mantle sections, but can be found in different tectonic settings throughout the world. They often occur as xenoliths in kimberlites and basalts (Lee and Rudnick, 1999; Beard et al., 2007; Rehfeldt et al., 2008) or in ultramafic sections of ophiolites (Koga et al., 2001) or in orogenic peridotite complexes (Holm and Praegel, 2006). Wehrlites with relatively Fe-rich compositions (mostly Fo<90) are typically interpreted to be high-pressure ultramafic cumulates derived from mafic–ultramafic melts trapped in the lower crustal depth, mostly related to the host magma (Frey and Prinz, 1978; Mattielli et al., 1996; Peltonen et al., 1999; Downes et al., 2007). An alternative explanation is that the wehrlites are the result of interaction between lherzolite and melt. The melt firstly replaced the primary spinel, cpx, and then the opx, and then crystallized as an assemblage of cpx + olivine + spinel, thereby changing the lherzolite modal composition towards that of the wehrlite suite (Xu et al., 1996b; Ionov et al., 2005).

The composition of cumulate xenoliths derived from lower crustal depth should, in general, range from ultramafic cumulates (dunite, wehrlite, and websterite) to gabbros. Gabbros have not been found in the Beiyan basalts. In addition, the olivines of the Beiyan wehrlites show undulatory extinction and kink bands which cannot be found in cumulates. The Beiyan wehrlites have extremely enriched major element compositions and show a trend with other lherzolites and cpx-rich lherzolites (Fig. 6) reflecting a sequential evolution from cpx-rich lherzolites during the interaction with melt. Additionally, the Beiyan wehrlites fall within the field of non-cratonic mantle peridotites, similar to the Shanwang peridotites and Daxizhuang composite xenolith, and far from the field of cumulates (Fig. 11a, c and d). In the plot of cpx Al^{IV} vs. Al^{VI}, the Beiyan wehrlites also fall within the field of xenoliths in basaltic rocks (Fig. 11b). Therefore, the Beiyan wehrlites are definitely not of cumulate origin.

Zhang et al. (2007a) show a composite xenolith comprising a lherzolite core, a sheared mantle and a reactant wehrlite rim against the Late Cretaceous host basalt in Daxizhuang, Jiaodong region. In addition, the sheared mantle mentioned above is also a wehrlite with the absence of opx. These features indicate that lherzolite can react with host basalt that originated in the asthenosphere to generate enriched wehrlite. This is exactly what we have observed in the Beiyan wehrlites, but we have not found the lherzolite with a rim of wehrlite. Thus, the Beiyan wehrlite should not be produced by lherzolite–host reaction, but should be produced from lherzolite protoliths through an interaction with asthenospheric melts. This melt first replaced the primary spinel, cpx, and then the low-Ca opx, as evidenced by rim replacement textures (Fig. 4a, b, d), and then crystallized as an assemblage of sieve-textured cpx, olivine and spinel, thereby changing the lherzolite suite towards the wehrlite suite.

6.3. Mantle metasomatism and the origin of the metasomatic agent

Petrological and geochemical characteristics of cpx-rich lherzolites and wehrlites provide unequivocal evidence for the existence of mantle metasomatism. The presence of phlogopite, amphibole and feldspar also indicates a metasomatic overprint. Trace element patterns from the Beiyan peridotites (Figs. 7 and 8) reflect multi-stage mantle processes. LREE enrichments in cpx (Figs. 7b, c and 8) mean that they have experienced later mantle metasomatism, while the spoon-shaped patterns (Fig. 7a) indicate a process of partial melting before chromatographic metasomatism by melt infiltration (Navon and Stolper, 1987). The convex-upward REE pattern (Fig. 7b) confirms that a secondary melt infiltration process is involved subsequent to partial melting since this type of pattern is diagnostic of equilibrium with LREE-rich melts (Navon and Stolper, 1987). The difference in trace element profiles between whole rock and cpx separates (Figs. 7 and 8) indicates that some trace elements reside elsewhere, perhaps in interstitial phases or in fluid inclusions in minerals.

In general, proposed metasomatic agents could include alkali-rich silicate (Wulff-pedersen et al., 1996) and CO_2–H_2O-rich fluids or carbonatite melts (Wiechert et al., 1997; Zangana et al., 1997; Coltorti et al., 1999).

The metasomatic signatures in the Beiyan peridotites are evident in enrichments in LREE (Figs. 7 and 8) and Sr (Fig. 12a). Although Beiyan peridotites contain hydrous minerals such as amphibole and phlogopite, these mineral are very rare and thus CO_2–H_2O-rich fluid is not the dominant metasomatic agent. Occurrence of apatite and calcite and positive Ba and Sr anomalies for the whole rock reflect carbonatitic metasomatism, consistent with cpx from wehrlite CLB05-01 which falls in the field of carbonatitic metasomatism (Fig. 12b). However, the cpxs of the dominant samples have low $(La/Yb)_N$ and high Ti/Eu ratios, suggesting mainly silicate metasomatism (Fig. 12b). Cpxs from two wehrlites (CLB05-35 and CLB05-80) have positive Ti anomalies. Rivalenti et al. (1996) pointed out that the apparent immobility of Ti during the metasomatic process in mantle peridotites could be due to the following reasons: reduced Ti solubility in hydrous fluids, fractionation of Ti-rich phases from percolating silicate melts, or

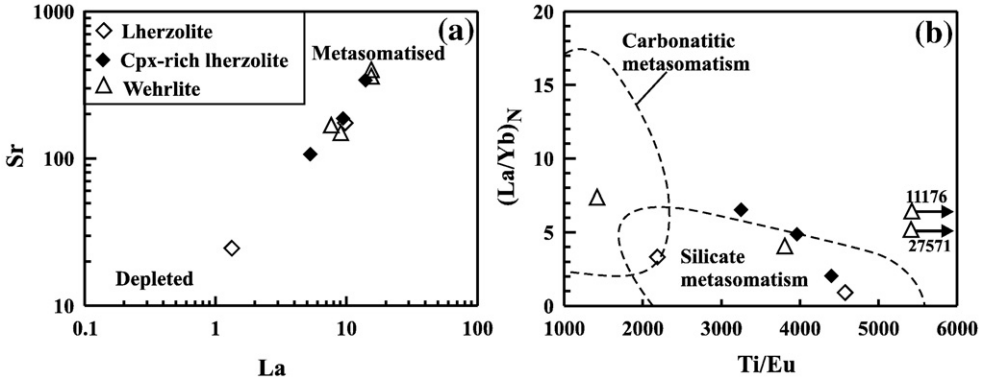

Fig. 12. Plots of La vs. Sr (a) and Ti/Eu vs. $(La/Yb)_N$ (b) in cpx from the Beiyan peridotites. Fields for "carbonatitic" and "silicate" metasomatism are after Coltorti et al. (1999).

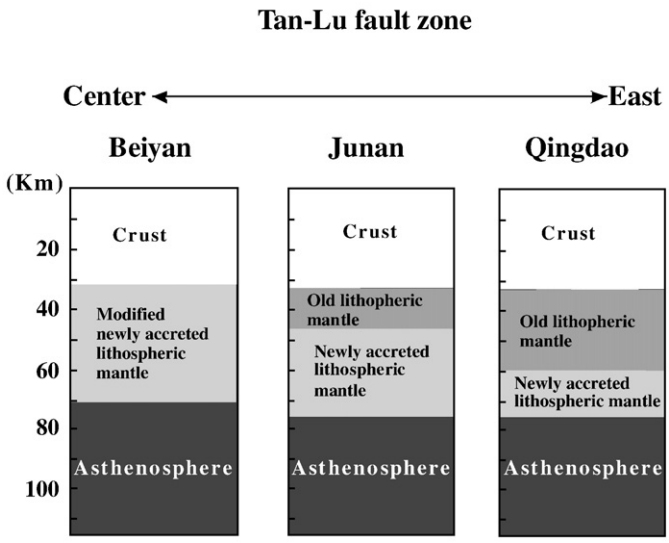

Fig. 13. Sketch map showing the lithospheric architecture beneath the Tan-Lu fault zone. The lithospheric architecture is inferred from the mineral and Sr–Nd isotopic compositions of the peridotite xenoliths from these localities.

reaction with carbonate-rich melts formerly equilibrated with amphibole peridotites.

The depleted Sr–Nd isotopic composition (Fig. 9) indicates that the reactant melt was mainly derived from an upwelling of the asthenosphere.

6.4. The role of Tan-Lu fault in the evolution of lithospheric mantle

Although both the Junan and Qingdao Late Mesozoic basaltic rocks contain two groups of peridotite xenoliths (high-Mg# (>91) and low-Mg# (≤91)), the percentages of the high-Mg# and low-Mg# peridotites vary from each other (Ying et al., 2006; Zhang et al., 2009b). The majority of the xenoliths from Qingdao are high-Mg#, with small amounts of low-Mg# peridotites and Archean lower crust granulites (Zhang and Zhang, 2007), while the xenoliths from Junan are mainly low-Mg# peridotites, with only one high-Mg# peridotite having been found, although there are abundant lower crust granulite xenoliths. If these xenoliths were randomly sampled from the lithospheric mantle during the ascent of the magmas, the Late Mesozoic–Cenozoic lithospheric profile in Shandong can be drawn (Fig. 13). The lithospheric mantle in Qingdao is composed of a small amount of newly accreted lithospheric mantle and dominant ancient lithospheric mantle which was substantially modified. The Junan lithospheric mantle is mainly composed of newly accreted lithospheric mantle, with only a small amount of ancient residue at the top of the upper mantle. All the peridotite xenoliths entrained in the Late Mesozoic basaltic rocks in Qingdao, Daxizhuang and Junan, eastern Shandong, are spinel-facies, and no garnet-facies xenoliths have been found, which indicates that the thickness of lithosphere is less than 75–80 km. This inference is consistent with the result of geophysical investigation of the Tan-Lu fault and its neighboring regions (Chen et al., 2006). The proximity of Junan to the Tan-Lu fault zone relative to Qingdao indicates that the Tan-Lu fault played an important role in the evolution of lithospheric mantle beneath the eastern NCC. The fault behaved as a conduit for melt ascent, resulting in a higher degree of lithospheric modification and thinning and larger amount of newly accreted lithosphere in the region proximal to the Tan-Lu fault.

The Beiyan basalts located within the Tan-Lu fault and their entrained peridotites are very low in their olivine Fo values (Fig. 10), among which the highest Fo value is close to that of Junan low-Mg# peridotites. This suggests that the lithospheric mantle beneath the Tan-Lu fault zone is composed of newly accreted lithospheric mantle, without the remnants of old lithospheric mantle (Fig. 13). Abundant cpx-rich lherzolites and wehrlites with extremely low Fo (<87) values also occur in the interior of Tan-Lu fault zone beside the Beiyan locality, such as Nüshan of Anhui Province (Xu et al., 1998), Shanwang of Shangdong Province (Zheng et al., 1998) and Fuxin of Liaoning Province (Zheng et al., 2007). Therefore, the Tan-Lu fault zone facilitates the ascent of asthenosphere and enhances the degree of peridotite–melt reaction. The lithospheric mantle beneath the Tan-Lu fault and its eastern part is heterogeneous (Fig. 13).

7. Conclusions

From the mineralogical, geochemical and isotopic studies of peridotites entrained in the Beiyan basalts within the Tan-Lu fault zone, the following conclusions can be drawn:

(1). The lithospheric mantle beneath Beiyan is composed of lherzolites, cpx-rich lherzolites and wehrlites. The dominant lherzolites represent fragments of newly accreted lithospheric mantle that makes up much of the Late Mesozoic–Cenozoic lithosphere beneath the Tan-Lu fault zone such as Junan, Qingdao and Shanwang. Shallow relics of the Archean cratonic mantle do not exist in this region because refractory peridotites are absent.

(2). The occurrence of cpx-rich lherzolites with low Fo (<87) and many wehrlites records important information on mantle processes, including textural and mineralogical evidence for a progressive metasomatic change in a sequence: lherzolite → cpx-rich lherzolite → wehrlite. Thus, the wehrlite suite at Beiyan originated from the interaction between the lherzolite mantle and an infiltrating metasomatic melt, rather than through igneous processes. The reactant melt was mainly derived from asthenosphere upwelling and was a carbonatitic silicate melt.

(3). The lithospheric mantle beneath the Tan-Lu fault and its eastern part is heterogeneous in time and space. The Tan-Lu fault zone might have acted as a major channel for asthenosphere upwelling and played an important role in the evolution of the sub-continental lithospheric mantle.

Acknowledgments

Authors would like to thank Mao Q., Ma Y.G., Chen F.K., and Chu Z.Y. for their assistance with the elemental and Sr–Nd isotopic analyses at the Institute of Geology and Geophysics, Chinese Academy of Sciences. This research was financially supported by the Chinese

Academy of Sciences (grant KZCX2-YW-103) and the Nature Science Foundation of China (grants 90714008; 40721062; 40523003). We thank Nelson Eby, Hilary Downes and an anonymous reviewer for their constructive reviews which greatly improved the quality of the manuscript.

References

Anders, E., Grevesse, N., 1989. Abundances of the elements: meteoritic and solar. Geochimica et Cosmochimica Acta 53, 197–214.

Aoki, K., Kushiro, I., 1968. Some clinopyroxenes from ultramafic inclusions in Dreiser Weiher, Eifel. Contributions to Mineralogy and Petrology 18, 326–337.

Beard, A.D., Downes, H., Mason, P.R.D., Vetrin, V.R., 2007. Depletion and enrichment processes in the lithospheric mantle beneath the Kola Peninsula (Russia): evidence from spinel lherzolite and wehrlite xenoliths. Lithos 94, 1–24.

Bodinier, J.L., Vasseur, G., Vernieres, J., Dupuy, C., Fabries, J., 1990. Mechanisms of mantle metasomatism — geochemical evidence from the lherz orogenic peridotite. Journal of Petrology 31, 597–628.

Boyd, F.R., 1989. Compositional distinction between oceanic and cratonic lithosphere. Earth and Planetary Science Letters 96, 15–26.

Boyd, F.R., Nixon, P.H., 1978. Ultramafic nodules from Kimberley pipes, South-Africa. Geochimica et Cosmochimica Acta 42, 1367–1382.

Cao, R.L., Zhu, S.H., 1987. Mantle Xenoliths and Alkaline Rich Host Rocks in Eastern China. In: Nixon, P.N. (Ed.), Mantle Xenoliths. John Wiley and Sons, Chichester, pp. 167–180.

Chen, D.G., Peng, Z.C., 1985. K–Ar ages and Pb, Sr isotopic characteristics of Cenozoic volcanic rocks in Shandong, China. Geochimica (Beijing) 4, 293–303 (in Chinese with English abstract).

Chen, L., Zheng, T.Y., Xu, W.W., 2006. A thinned lithospheric image of the Tan-Lu fault zone, eastern China: constructed from wave equation based receiver function migration. Journal of Geophysical Research-Solid Earth 111, B09312. doi:10.1029/2005JB003974.

Chi, J.S., Lu, F.X., 1996. Kimberlites and Palaeozoic Mantle beneath the North China Platform. Science Press, Beijing. (in Chinese).

Chu, Z.Y., Wu, F.Y., Walker, R.J., Rudnick, R.L., Pitcher, L., Puchtel, I.S., Yang, Y.H., Wilde, S.A., 2009. Temporal evolution of the lithospheric mantle beneath the Eastern North China craton. Journal of Petrology 50, 1857–1898.

Coltorti, M., Bonadiman, C., Hinton, R.W., Siena, F., Upton, B.G.J., 1999. Carbonatite metasomatism of the oceanic upper mantle: evidence from clinopyroxenes and glasses in ultramafic xenoliths of Grande Comore, Indian Ocean. Journal of Petrology 40, 133–165.

Downes, H., 1990. Shear zones in the upper mantle — relation between geochemical enrichment and deformation in mantle peridotites. Geology 18, 374–377.

Downes, H., 2001. Formation and modification of the shallow subcontinental lithospheric mantle: a review of geochemical evidence from ultramafic xenolith suites and tectonically emplaced ultramafic massifs western and central Europe. Journal of Petrology 42, 233–260.

Downes, H., Upton, B.G.J., Connolly, J., Beard, A.D., Bodinier, J.L., 2007. Petrology and geochemistry of a cumulate xenolith suite from Bute: evidence for late Palaeozoic crustal underplating beneath SW Scotland. Journal of the Geological Society of London 164, 1217–1231.

E, M.L., Zhao, D.S., 1987. The Cenozoic Basalts and Its Mantle Xenoliths in North of China. Science Publishing House, Beijing. (in Chinese).

Erlank, A.J., Waters, F.G., Hawkesworth, C.J., Haggerty, S.E., Allsopp, H.L., Richard, R.S., Menzies, M.A., 1987. Evidence for Mantle Metasomatism in Peridotite Nodules from the Kimberley Pipes, South Africa. In: Menzies, M.A., Hawkesworth, C.J. (Eds.), Mantle Metasomatism. Academic Press, London, pp. 221–311.

Fan, Q.C., Hooper, P.R., 1989. The mineral chemistry of ultramafic xenoliths of eastern China: implications for upper mantle composition and the paleogeotherms. Journal of Petrology 30, 1117–1158.

Fan, W.M., Zhang, H.F., Baker, J., Jarvis, K.E., Mason, P.R.D., Menzies, M.A., 2000. On and off the North China Craton: where is the Archaean keel? Journal of Petrology 41, 933–950.

Frey, F.A., Prinz, M., 1978. Ultramafic inclusions from San Carlos, Arizona: petrologic and geochemical data bearing on their petrogenesis. Earth and Planetary Science Letters 38, 129–176.

Griffin, W.L., Andi, Z., O'Reilly, S.Y., Ryan, C.G., 1998. Phanerozoic evolution of the lithosphere beneath the Sino-Korean Craton. Mantle Dynamics and Plate Interactions in East Asia 27, 107–126.

Griffin, W.L., O'Reilly, S.Y., Ryan, C.G., 1999. The Composition and Origin of Sub-Continental Lithospheric Mantle. In: Fei, Y., Mysen, B.O. (Eds.), Mantle Petrology: Field Observations and High-Pressure Experimentation: a Tribute to Francis R. (Joe) Boyd: In: Ber1tKa, C.M. (Ed.), The Geochemical Society Special Publication, Houston, pp. 13–45.

Harris, J.W., Duncan, D.J., Zhang, F., Miao, Q., Zhu, Y., 1994. The Physical Characteristics and Syngenetic Inclusion Geochemistry of Diamonds from Pipe 50, Liaoning province, People's Republic of China. In: Meyer, H.O.A., Leonardos, O.H. (Eds.), 5th International Kimberlites Conference, Brasilia, pp. 106–115.

Holm, P.M., Praegel, N.O., 2006. Cumulates from primitive rift-related East Greenland Paleogene magmas: petrological and isotopic evidence from the ultramafic complexes at Kaelvegletscher and near Kaerven. Lithos 92, 251–275.

Hu, S.B., He, L.J., Wang, J.Y., 2000. Heat flow in the continental area of China: a new data set. Earth and Planetary Science Letters 179, 407–419.

Ionov, D.A., Chanefo, I., Bodinier, J.L., 2005. Origin of Fe-rich lherzolites and wehrlites from Tok, SE Siberia by reactive melt percolation in refractory mantle peridotites. Contributions to Mineralogy and Petrology 150, 335–353.

Jin, L.Y., 1985. K–Ar ages of Cenozoic volcanic rocks in the middle segment of the Tan-Lu fault zone and stages of related volcanic activity. Geological Review 31, 309–315 (in Chinese with English abstract).

Koga, K.T., Kelemen, P.B., Shimizu, N., 2001. Petrogenesis of the crust–mantle transition zone and the origin of lower crustal wehrlite in the Oman ophiolite. Geochemistry Geophysics Geosystems 2 2000GC000132.

Lee, C.T., Rudnick, R.L., 1999. Compositionally Stratified Cratonic Lithosphere: Petrology and Geochemistry of Peridotite Xenoliths the Labait volcano, Tanzania. In: Gurney, J.J., Gurney, J.L., Ascoe, M.D. (Eds.), 7th International Kimberlite Conference. RedRoof Design, Cape Town, pp. 503–521.

Liu, D.Y., Nutman, A.P., Compston, W., Wu, J.S., Shen, Q.H., 1992. Remnants of 3800 Ma crust in the Chinese part of the Sino-Korean Craton. Geology 20, 1–20.

Mattielli, N., Weis, D., Grégoire, M., Mennessier, J.P., Cottin, J.Y., Giret, A., 1996. Kerguelen basic and ultrabasic xenoliths: evidence for long-lived Kerguelen hotspot activity. Lithos 37, 261–280.

McDonough, W.F., Stosch, H.G., Ware, N.G., 1992. Distribution of titanium and the rare earth elements between peridotitic minerals. Contributions to Mineralogy and Petrology 110, 321–328.

Menzies, M.A., Fan, W.M., Zhang, M., 1993. Palaeozoic and Cenozoic Lithoprobes and the Loss of 120 km of Archaean Lithosphere, Sino-Korean Craton, China. In: Prichard, H.M., Alabaster, T., Harris, N.B.W., Neary, C.R. (Eds.), Magmatic Processes and Plate Tectonics: Geological Society Special Publication, pp. 71–81.

Menzies, M.A., Xu, Y.G., Zhang, H.F., Fan, W.M., 2007. Integration of geology, geophysics and geochemistry: a key to understanding the North China Craton. Lithos 96, 1–21.

Meyer, H.O.A., Zhang, A., Milledge, H.J., 1994. Diamonds and Inclusions in Diamonds from Chinese Kimberlites. In: Meyer, H.O.A., Leonardos, O.H. (Eds.), 5th International Kimberlite Conference, Brasilia, pp. 98–105.

Navon, O., Stolper, E., 1987. Geochemical consequences of melt percolation: the upper mantle as a chromatographic column. Journal of Geology 95, 285–307.

O'Reilly, S.Y., Griffin, W.L., Poudjom, Y.H., Morgan, P., 2001. Are lithophere forever? Tracking changes in subcontinental lithospheric mantle through time. GSA Today 11, 4–10.

Pearson, D.G., 1999. The age of continental roots. Lithos 48, 171–194.

Peltonen, P., Huhma, H., Tyni, M., Shimizu, N., 1999. Garnet Peridotite Xenoliths from Kimberlites of Finland: Nature of the Continental Mantle at an Archaean craton-Proterozoic Mobile Belt Transition. Proceedings of 7th International Kimberlite Conference. Red Roof Design, Cape Town, South Africa, pp. 664–676.

Peng, Z.C., Zartman, R.E., Futa, K., Chen, D.G., 1986. Pb-isotopic, Sr-isotopic and Nd-isotopic systematics and chemical characteristics of Cenozoic basalts, eastern China. Chemical Geology 59, 3–33.

Pouchou, J.L., Pichoir, F., 1991. Quantitative Analysis of Homogeneous or Stratified Microvolumes Applying the Model "PAP". In: Heinrich, K.F.J., Newbury, D.E. (Eds.), Electron Probe Quantification. Plenum, New York, pp. 31–75.

Rampone, E., Bottazzi, P., Ottolini, L., 1991. Complementary Ti and Zr anomalies in orthopyroxene and clinopyroxene from mantle peridotites. Nature 59, 472–489.

Rehfeldt, T., Foley, S.F., Jacob, D.E., Carlson, R.W., Lowry, D., 2008. Contrasting types of metasomatism in dunite, wehrlite and websterite xenoliths from Kimberley, South Africa. Geochimica et Cosmochimica Acta 72, 5722–5756.

Rivalenti, G., Vannucci, R., Rampone, E., Mazzucchelli, M., Piccardo, G.B., Piccirillo, E.M., Bottazzi, P., Ottolini, L., 1996. Peridotite clinopyroxene chemistry reflects mantle processes rather than continental versus oceanic settings. Earth and Planetary Science Letters 139, 423–437.

Rudnick, R.L., Shan, G., Ling, W.L., Liu, Y.S., McDonough, W.F., 2004. Petrology and geochemistry of spinel peridotite xenoliths from Hannuoba and Qixia, North China craton. Lithos 77, 609–637.

Sun, S.S., McDonough, W.F., 1989. Chemical and Isotopic Systematic of Oceanic Basalt: Implication for Mantle Composition and Processes. In: Saunders, A.D., Norry, M.J. (Eds.), Magmatism in the Oceanic Basins: Geological Society of London, Special Publication, pp. 313–346.

Tang, Y.J., Zhang, H.F., Ying, J.F., 2006. Asthenosphere–lithospheric mantle interaction in an extensional regime: implication from the geochemistry of Cenozoic basalts from Taihang Mountains, North China Craton. Chemical Geology 233, 309–327.

Tang, Y.J., Zhang, H.F., Ying, J.F., Zhang, J., Liu, X.M., 2008. Refertilization of ancient lithospheric mantle beneath the central North China Craton: evidence from petrology and geochemistry of peridotite xenoliths. Lithos 101, 435–452.

Walter, M.J., 2003. Melt Extraction and Compositional Variability in Mantle Lithosphere. In: Carlson, R.W. (Ed.), The mantle and core. Carnegie Institution of Washington, Treatise on Geochemistry, Washington, DC, pp. 363–394.

Wang, W.Y., Gasparik, T., 2001. Metasomatic clinopyroxene inclusions in diamonds from the Liaoning province, China. Geochimica et Cosmochimica Acta 65, 611–620.

Wang, F.Z., Jin, L.Y., Xu, Y.R., 1987. The study of ultramafic inclusions in Cenozoic basalt in Linqu of Shandong. Earth Science 12 (3), 249–256 (in Chinese with English abstract).

Wang, S.Y., Liu, M.W., Liang, B.Q., 2003. New discovery of Cenozoic volcanic craters and its significance of tourism and geology in Changle County, Shandong Province. Land and Resource of Shandong Province 8, 48–50 (in Chinese with English abstract).

Wiechert, U., Ionov, D.A., Wedepohl, K.H., 1997. Spinel peridotite xenoliths from the Atsagin-Dush volcano, Dariganga lava plateau, Mongolia: a record of partial melting and cryptic metasomatism in the upper mantle. Contributions to Mineralogy and Petrology 126, 345–364.

Wulff-pedersen, E., Neumann, E.R., Jensen, J.J., 1996. The upper mantle under La Palma, Canary Islands: formation of Si–K–Na-rich melt and its importance as a metasomatic agent. Contributions to Mineralogy and Petrology 125, 113–139.

Xu, Y.G., 2001. Thermo-tectonic destruction of the archaean lithospheric keel beneath the Sino-Korean Craton in China: evidence, timing and mechanism. Physics and Chemistry of the Earth Part a-Solid Earth and Geodesy 26, 747–757.
Xu, J.W., Zhu, G., Tong, W.X., Cui, K.R., Liu, Q., 1987. Formation and evolution of the Tancheng-Lujiang wrench fault system: a major shear system to the northwest of the Pacific Ocean. Tectonophysics 134, 273–310.
Xu, Y.G., Ross, J.V., Mercier, J.C.C., 1993. The upper-mantle beneath the Continental Rift of Tan-Lu, eastern China — evidence for the intra-lithospheric shear zones. Tectonophysics 225, 337–360.
Xu, Y.G., Menzies, M.A., Mattey, D.P., Lowry, D., Harte, B., Hinton, R.W., 1996a. The nature of the lithospheric mantle near the Tancheng-Lujiang fault, China: an integration of texture, chemistry and O-isotopes. Chemical Geology 134, 67–81.
Xu, Y.G., Mercier, J.C.C., Menzies, M.A., Ross, J.V., Harte, B., Lin, C.Y., Shi, L.B., 1996b. K-rich glass-bearing wehrlite xenoliths from Yitong, northeastern China: petrological and chemical evidence for mantle metasomatism. Contributions to Mineralogy and Petrology 125, 406–420.
Xu, X.S., O'Reilly, S.Y., Griffin, W.L., Zhou, X.M., Huang, X.L., 1998. The Nature of the Cenozoic Lithosphere at Nüshan, Eastern China. In: Flower, M.F.J., Chung, S.J., Lo, C.H., Lee, T.Y. (Eds.), Mantle Dynamics and Plate Interactions in East Asia: American Geophysical Union, Geodynamics Series, pp. 167–195.
Zhou, X.H., Armstrong, R.L., 1982. Cenozoic volcanic-rocks of eastern China — secular and geographic trends in chemistry and strontium isotopic composition. Earth and Planetary Science Letters 58, 301–329.
Xu, X.S., O'Reilly, S.Y., Griffin, W.L., Zhou, X.M., 2000. Genesis of young lithospheric mantle in southeastern China: an LAM-ICPMS trace element study. Journal of Petrology 41, 111–148.
Yan, J., Chen, J.F., Xie, Z., Zhou, T.X., 2003. Mantle derived xenoliths in the late Cretaceous basalts in eastern Shandong: new constraints on the timing of lithospheric thinning in east China. Chinese Science Bullutin 48, 1570–1574.
Yang, W., Teng, F.Z., Zhang, H.F., 2009. Chondritic magnesium isotopic composition of the terrestrial mantle: a case study of peridotite xenoliths from the North China craton. Earth and Planetary Science Letters 288, 475–482.
Ying, J.F., Zhang, H.F., Kita, N., Morishita, Y., Shimoda, G., 2006. Nature and evolution of late cretaceous lithospheric mantle beneath the eastern North China Craton: constraints from petrology and geochemistry of peridotitic xenoliths from Junan, Shandong Province, China. Earth and Planetary Science Letters 244, 622–638.
Zangana, N.A., Downes, H., Thirlwall, M.F., Hegner, E., 1997. Relationship between deformation, equilibration temperatures, REE and radiogenic isotopes in mantle xenoliths (Ray Pic, Massif Central, France): an example of plume-lithosphere interaction? Contributions to Mineralogy and Petrology 127, 187–203.
Zhang, H.F., 2005. Transformation of lithospheric mantle through peridotite–melt reaction: a case of Sino-Korean craton. Earth and Planetary Science Letters 237, 768–780.
Zhang, H.F., Sun, M., 2002. Geochemistry of Mesozoic basalts and mafic dikes, southeastern North China Craton, and tectonic implications. International Geology Review 44, 370–382.
Zhang, H.F., Yang, Y.H., 2007. Emplacement age and Sr–Nd–Hf isotopic characteristics of the diamondiferous kimberlites from the eastern North China Craton. Acta Petrologica Sinica 23 (2), 285–294 (in Chinese with English abstract).
Zhang, J., Zhang, H.F., 2007. Compositional features and P–T conditions of granulite xenoliths from late Cretaceous mafic dike, Qingdao region. Acta Petrologica Sinica 23, 1133–1140 (in Chinese with English abstract).
Zhang, H.F., Sun, M., Zhou, X.H., Fan, W.M., Zhai, M.G., Ying, J.F., 2002. Mesozoic lithosphere destruction beneath the North China Craton: evidence from major, trace element, and Sr–Nd–Pb isotope studies of Fangcheng basalts. Contributions to Mineralogy and Petrology 144, 241–253.
Zhang, H.F., Sun, M., Zhou, X.H., Zhou, M.F., Fan, W.M., Zheng, J.P., 2003. Secular evolution of the lithosphere beneath the eastern North China Craton: evidence from Mesozoic basalts and high-Mg andesites. Geochimica et Cosmochimica Acta 67, 4373–4387.
Zhang, H.F., Sun, M., Zhou, M.F., Fan, W.M., Zhou, X.H., Zhai, M.G., 2004. Highly heterogeneous Late Mesozoic lithospheric mantle beneath the North China Craton: evidence from Sr–Nd–Pb isotopic systematics of mafic igneous rocks. Geological Magazine 141, 55–62.
Zhang, H.F., Sun, M., Zhou, X.H., Ying, J.F., 2005. Geochemical constraints on the origin of Mesozoic alkaline intrusive complexes from the North China Craton and tectonic implications. Lithos 81, 297–317.
Zhang, H.F., Nakamura, E., Kobayashi, K., Zhang, J., Ying, J.F., Tang, Y.J., Niu, L.F., 2007a. Transformation of subcontinental lithospheric mantle through deformation-enhanced peridotite–melt reaction: evidence from a highly fertile mantle xenolith from the North China craton. International Geology Review 49, 658–679.
Zhang, H.F., Ying, J.F., Shimoda, G., Kita, N.T., Morishita, Y., Shao, J.A., Tang, Y.J., 2007b. Importance of melt circulation and crust–mantle interaction in the lithospheric evolution beneath the North China Craton: evidence from Mesozoic basalt-borne clinopyroxene xenocrysts and pyroxenite xenoliths. Lithos 96, 67–89.
Zhang, H.F., Goldstein, S.L., Zhou, X.H., Sun, M., Zheng, J.P., Cai, Y., 2008. Evolution of subcontinental lithospheric mantle beneath eastern China: Re–Os isotopic evidence from mantle xenoliths in Paleozoic kimberlites and Mesozoic basalts. Contributions to Minerology and Petrology 155, 271–293.
Zhang, H.F., Goldstein, S., Zhou, X.H., Sun, M., Cai, Y., 2009a. Comprehensive refertilization of lithospheric mantle beneath the North China Craton: further Os–Sr–Nd isotopic constraints. Journal of the Geological Society of London 166, 1–11.
Zhang, J., Zhang, H.F., Kita, N., Shimoda, G., Morishita, Y., Ying, J.F., Tang, Y.J., 2009b. Secular evolution of the lithospheric mantle beneath the eastern North China craton: evidence from peridotitic xenoliths from Late Cretaceous mafic rocks in the Jiaodong region, east-central China. International Geology Review. doi:10.1080/00206810903025090.
Zhao, G.C., Wilde, S.A., Cawood, P.A., Sun, M., 2001. Archean blocks and their boundaries in the North China Craton: lithological, geochemical, structural and P–T path constraints and tectonic evolution. Precambrian Research 107, 45–73.
Zhao, X.M., Zhang, H.F., Zhu, X.K., Zhang, W.H., Yang, Y.H., Tang, Y.J., 2007. Metasomatism of Mesozoic and Cenozoic lihtospheric mantle beneath the North China Craton: evidence from phlogopite-bearing mantle xenoliths. Acta Petrologica Sinica 23, 1281–1293 (in Chinese with English abstract).
Zheng, J.P., O'Reilly, S.Y., Griffin, W.L., Lu, F.X., Zhang, M., 1998. Nature and evolution of Cenozoic lithospheric mantle beneath Shandong peninsula, Sino-Korean Craton, eastern China. International Geology Review 40, 471–499.
Zheng, J.P., O'Reilly, S.Y., Griffin, W.L., Lu, F.X., Zhang, M., Pearson, N.J., 2001. Relict refractory mantle beneath the eastern North China block: significance for lithosphere evolution. Lithos 57, 43–66.
Zheng, J.P., Griffin, W.L., O'Reilly, S.Y., Yu, C.M., Zhang, H.F., Pearson, N., Zhang, M., 2007. Mechanism and timing of lithospheric modification and replacement beneath the eastern North China Craton: peridotitic xenoliths from the 100Ma Fuxin basalts and a regional synthesis. Geochimica et Cosmochimica Acta 71, 5203–5225.
Zindler, A., Hart, S., 1986. Chemical geodynamics. Annual Review of Earth Planetary Science 14, 493–571.